Nanoscale

ROYAL SOCIETY OF CHEMISTRY

REVIEW

Cite this: *Nanoscale*, 2021, **13**, 2113

Liquid metal-based nanocomposite materials: fabrication technology and applications

Nyamjargal Ochirkhuyag, Ryosuke Matsuda, Zihao Song, Fumika Nakamura, Takuma Endo and Hiroki Ota *

Received 19th October 2020,
Accepted 17th December 2020

DOI: 10.1039/d0nr07479a

rsc.li/nanoscale

Research on liquid metals has been steadily garnering more interest in recent times, especially in flexible electronics applications because of their properties like possessing high conductivity and being liquid state at room temperature. The unique properties afforded by such materials at low temperatures can compensate for the limitations of stretchable electronic devices, particularly robustness and their fluidic property, which can enhance the flexibility and deformation of these devices. Therefore, interest in liquid-metal nanoparticles and liquid metals with nanocomposites has enabled research into their fabrication technologies as well as utilisation in fields such as chemistry, polymer engineering, computational modelling, and nanotechnology. In particular, in flexible and stretchable electronic device applications, the research attention is focused on the fabrication methodologies of liquid-metal nanoparticles and liquid metals containing nanocomposites. This review attempts to summarise the available stretchable and flexible electronics applications that use liquid-metal nanoparticles as well as liquid metals with nanomaterial additives.

Introduction

Over the past few years, liquid metal (LM) has been steadily attracting more interest, particularly in the flexible and soft electronics field and the related applications. The term 'Liquid metals' can be defined differently as numerous research efforts have been undertaken to use them in various applications and fields. The simplest definition for this term can be given as 'eutectic metals', which have the lowest melting points around 15 °C below room temperature, or 'Field's metals', which have melting point at 62 °C; these have good electrical and thermal conductivities because of change in mechanical properties at room temperature due to phase change'.[1] In addition to their uses in the soft electronics field, LMs are gaining attention in the medical engineering field, where they are commonly used in drug delivery. LMs can be used as nanoparticles or as nanocomposite materials in which other materials are used as additives. Liquid metal nanoparticles (LMNPs) and liquid metal nanocomposites (LMNCs) can be described as 'low melting point metals in nanoscale' and 'liquid metal with a combination of other metals' respectively. Researchers are gradually shifting their focus toward the use of LM-based materials to enhance the electrical properties (*e.g.*, the electric, dielectric, and thermal properties) of flexible and wearable electronics applications.[2] The technique of fabricating a stretchable conductor using an LM has been in use for a while now; traditionally, this method involves injecting mercury into a stretchable channel.[3] However, because of its high toxicity and high vapor pressure, mercury is not used widely, and product development with mercury is considered to be difficult. In contrast, Ga-based LMs at room temperature appear to be promising functional materials with low toxicities, low vapor pressures, high thermal conductivities, incomparable conductivity and deformability, and the ability to withstand high levels of mechanical deformation, which renders them well suited to fabricating stretchable electronics.[4–7] By combining them with other nanomaterials, the properties of LMs can be enhanced or even supplemented by new properties. Nanoscale mixtures of LMs with nanocomposite materials are well suited to applications in soft electronics and, because they would be easier to fabricate and pattern, to various applications using printing techniques such as inkjet and screen printing. As such materials remain in a liquid state even below their freezing temperatures, they are easier to deform or shape to meet various applicational designs, enabling reductions in device size. When LMs with elastomer nanocomposite materials are used to develop sensors, energy-harvesting transducers, and actuators, the electrical permittivity of the elastomer material is enhanced without decreasing its stretchable and flexibility.[8] The LMNCs are either LM

Yokohama National University, 79-5 Tokiwadai, Hodogaya-ku, Yokohama 240-8501, Japan

mixed with metallic nanoparticles or nanoscale droplets of LM that represent an important step towards utilising LM for soft electronic applications.[2]

Furthermore, the oxide layer/passivating oxide is essential to the discussion of LMNCs. The LM oxide layer/passivating oxide, which is generally removed to ensure high conductivity, prevents LMNPs from coalescing back into the bulk;[9] this mechanically stabilizes the nonequilibrium shape of the LMNPs, enabling fine metal patterning using printing techniques[10] while maintaining a reduced metal surface tension.[11] Despite its necessity in reconfigurable applications, however, the oxide layer increases the LMNPs' viscosity by sticking to the surfaces of other materials.[12] Even though the oxide layer needs to be removed, it is an important to the properties of LM, for instance, eutectic gallium–indium (EGaIn) because it increases the surface/volume ratio significantly, enabling adsorption of the LM onto a higher fraction of the nanoparticles. The Cabrera–Mott oxidation mechanism, which is the only probable mechanism for oxide development in gallium alloys, can be described as a 'low temperature oxidation based on the assumption that cation migration occurs under the influence of potential built up across the growing oxide film'.[13] This theory also accounts for the nanoparticle oxidation mechanism in other group III metals. The oxide growth process is driven by the presence of an electric field generated by the production of new surface states through the adsorption of O_2 onto the particle surfaces. The intensity of the resulting electrical potential is equal to the difference between the work function of the metal and the 2p energy level of the O. Thiols, or adsorbed molecules, can affect the measured work and change the dynamics of O_2 adsorption. The oxide layer or passivating oxide is a dynamic continuum emergent from the bulk and the result of an equilibrating system. The establishment of the passivating oxide is dependent on the environment and reactivity of the alloy components and is determined by the energy density, diffusivity, and thermodynamic state of the bulk. When formed properly, the passivating oxide or oxide layer can be advantageous to the material properties, improving, for example, the stability of undercooled liquid metal core–shell (ULMCS) particles, which in turn enables heat-free solders and a variety of other ambient or low-temperature metal processes dependent on the effects of free energy.[14] Studies of the oxide layers of Ga, In, galinstan, and EGaIn liquid metals have revealed that oxide layers form on metallic surfaces following exposure to oxygen. Although the oxide layers that form on Ga are passivating, those forming on indium are not. The thickness of the oxide layer is related to oxygen-exposure conditions such as the vacuum condition, relative humidity, temperature range, and pressure.[15]

The remainder of this review will focus on the usage of LMs in soft and flexible electronics and their applications. We discuss the property changes of LMs at the nanoscale level with and without additional composite materials. Then, we explain the main uses of LMs at the nanoscale level and their applications. The focus of this review is on soft, flexible, and stretchable electronics as these devices are rapidly gaining attention in current research. Fig. 1 shows the methods used to fabricate LMNPs and LMNCs (Fig. 1a-i, -ii, -iii, -iv), images of LM-based composites (Fig. 1b-i, -ii), patterning techniques (Fig. 1c-i, -ii), and related applications (Fig. 1d-i, -ii, -iii). The figure conveys the primary structure of this paper and can be referred to for further clarification of the following sections.

Liquid-metal nanocomposite materials

In general, LMNCs comprise LMs in the form of nanoparticles mixed with other nanostructure materials; by contrast, LMNPs are synthesised from bulk metals that have low melting points. The properties of the LM may be improved by the addition of other materials based on specific applications. LMs mixed with silicon nanoparticles have been demonstrated as battery anodes; the combination was observed to improve the electrochemical and mechanical performances, particularly stability. If the LM is mixed with polydimethylsiloxane (PDMS), Ecoflex, or other polymer materials, it is possible to apply soft electronic designs to achieve soft device applications.[26] Wearable sensing gloves that can successfully track human hand movements are typically fabricated using soft-matter capacitive sensors made of LMs with silicon elastomers.[27] Thus, LM nanoparticles (LMNPs) and LMNCs can be described from the perspective of fabrication techniques and material types that are currently in use. When discussing fabrication, the intermetallic interface should be mentioned. This interface forms as a result of the incomplete solid solubility of an alloy system. It has been reported that, in LM particle mixtures prepared *via* wet processing, the liquid or solid metal surfaces develop passivating oxide layers through contact with the air. To enable reactive wetting, such layers should be broken when they form on the surfaces of LM and Cu particles. To achieve intermetallic contact, oxide layers can be broken by inducing an electrical polarisation in the NaCl solution.[28] Potential/feasible materials for use in LMNPs include Li (lithium)-, Na (sodium)-, and K (potassium)-based alkali metals because of their usefulness as high-specific-volume anode materials and low redox potentials. However, batteries based on these alkali metals face safety issues, short circuit problems, and short lifespans, and further research is required. LMNCs can be based on low-melting-point metals such as Ca (calcium), Co (cobalt), Sr (strontium), and Cr (chromium). In addition to being highly soluble in Ga-LM, these metals have low melting points that can be further reduced by mixing them with LMNPs. Further developments using these materials based on the unique properties of LMs and refinements in metal systems are expected.

Liquid-metal nanoparticles

'LMNPs can be categorized as single or mixed depending on their concentrations and phases. The single LMNPs are composed of post-transition elements, zinc-group elements, and alkali metals (summarised in Table 1). As for mixed LMNPs, they can be intermixed to form alloys with a net melting

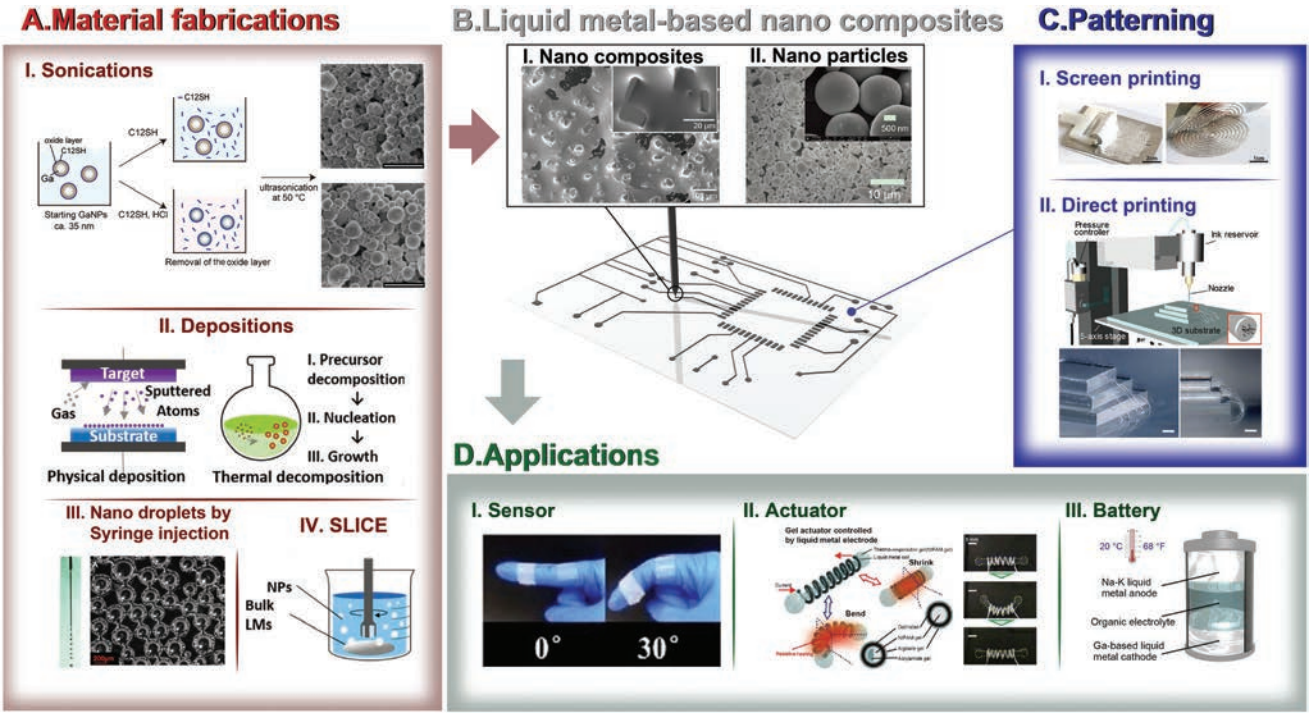

Fig. 1 Liquid metal-based methodologies for the fabrication of soft electronics: (a) material fabrication: (i) sonication;[16] (ii) deposition (PVD),[17] (iii) nanodroplets *via* syringe injection;[18] (iv) shear liquid into complex particles (SLICE).[17] (b) Liquid metal-based nanocomposites: (i) nanocomposites—liquid metal in which small tetragonal blocks[19] have formed; (ii) nanoparticles—SEM images of non-coalesced LMNPs.[20] (c) Patterning: (i) screen printing—image of Ni–GaIn applied to Ecoflex using a rolling brush;[21] (ii) direct printing—schematic of 3D direct printing system and composites printed onto soft 3D substrate (scale bar = 100 μm).[22] (d) Applications: (i) flexible sensor with strain angle;[23] (ii) hydrogel spring actuator;[24] (iii) room-temperature LM battery.[25]

Table 1 Liquid metal particle constituent elements[12,29,41]

		Melting point (°C)	Electrical conductivity (S m^{-1})	Thermal conductivity (W m^{-1} K^{-1})
Post transition metal	Ga (gallium)	29.8	7.1×10^6	29
	In (indium)	156.6	1.2×10^7	82
	Tl (thallium)	449.5	6.7×10^6	46
	Sn (tin)	231.9	9.1×10^6	67
	Pb (lead)	327.5	4.8×10^6	35
	Bi (bismuth)	271.4	7.7×10^5	8
Zinc group	Zn (zinc)	419.5	1.7×10^7	120
	Cd (cadmium)	321.1	1.4×10^7	96
	Hg (mercury)	−38.8	1×10^6	8.3
Alkali metal	Rb (rubidium)	39.31	8.3×10^6	58
	Cs (caesium)	28.44	5×10^6	36
	Fr (francium)	—	—	—
	EGaIn (eutectic Ga–In)	15.4	3.4×10^6	26.6
	Galinstan	13.2	3.46×10^6	16.5

point below 300 °C'.[29] In nanoscale applications, sonication and shearing techniques are commonly used to synthesise LMNPs; the sizes of the LMNPs fabricated *via* sonication can be adjusted. For example, the reversible size control of Ga LMNPs fabricated by controlling the power and temperature of ultrasonication to produce 35 nm particles at low temperatures and 60 nm particles at high temperatures has been reported. Furthermore, the size and number of particles are dependent on the sonication duration: longer processes produce smaller and higher number of particles.[16] High temperature and high pressure are generated locally, which form bubbles that burst within the LM; this is a convenient and easy-to-use method. Appropriate addition of surfactants allows the formation of self-assembled monolayers (SAMs) on the particle surfaces to effectively reduce coalescence between the LM particles.[30] Ultrasonication processes can

break LMs down to nanoparticles in less time (60 min) than shear liquid into complex particle (SLICE) processes, which can take around 120 min.[16,31,32] Sonication techniques (Fig. 1a-i) can be used to control the sizes of LMNPs by adjusting the temperature and speed.[16] The shapes of particles can be adjusted by tuning the solution concentration, sonication period, and temperature.[33] A mini ultrasonic platform device has been used to produce steady EGaIn nanoparticles with polymers in an aqueous solution through the application of a potential of 24 V for 20 min.[9] By contrast, the SLICE technique applies a rotary tool at a specific speed and for a specific duration to reduce the shear bulk of LM into particles in an acetic solution.[34] In this manner, SLICE (Fig. 1a-iv) can be used to process LMs into desired particles with an oxidation solution and an organic layer with a smooth surface as the second layer. Nanosized materials can be coated around LMNPs to create core–shell structures, and stable undercooled field metal and eutectic Bi–Sn alloy particles can be produced using the SLICE method.[34] Furthermore, undercooled LMs, which have metastability, are known to be compatible with complex fabrication routes and engineering. Even though they have low yields and poor stability, stable undercooled field metal particles and eutectic Bi–Sn alloys have been successfully produced using the SLICE technique.[35] Post-SLICE etching can be used to produce contacts between pairs of particles and release undercooled liquid cascades through particle beds, leading to the creation of point contacts and solidification through a process known as coalescence of undercooled particles through chemical trigger (CUPACT). Because it does not apply the capillary force necessary to break the particle shells, the CUPACT process retains particle sphericity, with intermetallic interfaces formed through the CUPACT process applied to the overlaying particles during surface soldering. As CUPACT is concentration dependent, the etching concentration dictates the properties of the resulting film. CUPACT films with resistivities of 63 μΩ have been fabricated, and it has been noted that the specific thermal conductivities of these films are very similar to that of the Bi–In–Tn bulk Field metal (2.4×10^{-3} W m^2 g^{-1} K^{-1}).[36] Undercooled liquid metal particles (ULMPs) have the unique properties of being liquid below their freezing temperatures and having metastability. They can also be used as self-stiffening composites, with mechanically induced stiffening and strengthening achieved through the triggering of polymerisation or cross-linking of polymer chains. A potential approach to transitioning from a triggering mechanism to a thermodynamical process is to embed metastable materials into the matrix; as a result, the metastable states of ULMPs can be used to overcome the complexity of fabrication. These types of materials can demonstrate specific property changes when externally triggered.[37] Electronical conductive interconnects based on ULMPs have been demonstrated. When a normal stress is applied to ULMPs, a predominantly surface deformation results.[36] The porous network of metallic interconnects produced by the delayed heat-free solidification enables efficient fluid diffusion while offering stable conductive traces, even on substrates with mismatched surface energies. To achieve the ambient fabrication of interconnected networks within a field metal, a minimum of 0.11 degrees of undercooling is required.[38] Microfluidic channels have been produced using stiffness tuning through thermodynamics relaxation (ST3R), an excellent platform for fabricating microfluidic channels based on its ability to produce instant, precision prototyping and rapidly fabricated complex designs. Low-melting-temperature metals or undercooled liquid metals can be used to produce reconfigurable channels by re-melting the metals to partly revert them to the intended shapes.[39] ULMPs have been used to demonstrate the possibility of soft lithography of lift-off materials with enhanced moduli, stiffnesses, and solvent insensitivity without damaging the delicate substrate. ULMPs have also been successfully used to produce close analogues of metallic rose surfaces.[40]

Liquid-metal nanocomposites

LMNC materials can be divided into three groups in terms of the additive material types used: (1) LM–polymer nanocomposites, (2) LMNPs comprising carbon nanotube (CNT) or CNT-related materials, and (3) LMNP–metal particle composites.[2] Adding other materials to LM enhances its properties or produces new properties; for example, adding iron (Fe) to the LM gives it magnetic properties, adding Cu provides remarkably high electroconductivity and thermal conductivity, and adding magnesium (Mg) enhances photothermal functionality. However, certain LM properties, including rigidity, conductivity, and adhesion, can also be derived as effects depending on the doping ratios of the particles. Metals such as gold (Au) and silver (Ag) are generally deposited onto LM droplets as an outer layer to form core–shell biphasic LMNCs. The new biphasic LM–Au composites can be sintered to form conductive traces for flexible circuits.[2] The common additive materials used with LMNCs are listed in Table 2, in which they are categorised in terms of the corresponding properties (electrical conductivity and magnetic and mechanical properties) useful for developing soft, flexible, and stretchable electronics.

The physical vapour deposition (PVD) and nanodroplet techniques can be used to fabricate LMNPs and LMNCs. Gallium–Indium (Ga–In) LMNPs are fabricated by PVD, where the process is completed in a vacuum chamber. The EGaIn is placed within a tungsten boat to provide the Ga and In sources. Under resistive heating, the EGaIn alloys are vaporised into Ga and In atoms, which diffuse towards and condense on the cold target substrate that is placed 25 cm above the heater. Accordingly, the particle sizes can be controlled, and LMNPs and LMNCs can be fabricated on various substrates by PVD (Fig. 1a-ii).[48] The Ga-LM droplet material is fabricated using the nanodroplet technique (Fig. 1a-iii), where a syringe filled with the LM is used to inject the LM into a Petri dish containing water and sodiumdodecylsulfate (SDS) to fabricate large LM droplets rapidly.[18]

Table 2 Common LMNC materials and their properties[22,29,42–47]

		Density (g cm^{-3})	Electrical conductivity (S m^{-1})	Enhancements of using LMNCs
Electrical conductivity	Au[44]	19.3	4.5×10^7	Increase compressive stress by lattice constant increase from 4.08 Å (Au) to 6.08 Å (Ga–Au)
	Ag[45]	9.32	6.2×10^7	Volumetric conductivity increased from 3.6 to 4.85×10^6 S m^{-1} $\times 10^6$ increase in electrical conductivity and 80% strain with low resistance (around 0 Ω)
Magnetic property	Ni[43]	8.908	1.4×10^7	Ni-LMNPs can be patterned on supermetallophobic substrates such as paper and PDMS by a permanent magnet
	Gd[42]	7.901	7.7×10^5	Crystallization temperature reduced from −14.3 to 024.6 °C. Also, Gd with galinstan LM demonstrated soft ferromagnetic properties like pure Gd Reversible magnetocaloric effect of Gd; S_m = 9 J kg^{-1} K^{-1} is observed
	Fe[46]	7.874	1×10^7	Magnetic LM can be stretched up to 46 mm but MLMD (magnetic LM droplet) increases stretchability up to 400% (1.5 mL of magnetic LM droplet)
Mechanical property	Pt[47]	21.45	9.4×10^6	The Pt is composed with LMEE. Its thermal conductivity is 4.7 W m^{-1} K^{-1}, which is 25 times greater than that of elastomer
	CNT[22]	—	—	Composite is printed with high conductivity up to 3×10^{-6} S m^{-1}, and high resolutions Thermal conductivity increases from 18.4 to 21 W m^{-1} K^{-1} as wt% of CNT increases

Patterning of liquid-metal-based materials for applications

The patterning techniques generally used can be classified under lithography, microchannels, direct laser patterning, and microcontact printing. Thus, the parameters required for patterning are the resolution of printing, adhesion, contact between LM and other materials, scalability, and deformability, among others.[49] This section focuses on the patterning of LMNP and LMNC materials as well as on the use of semi-LM paste. Various patterning techniques and their device applications are discussed individually. When combined with nanostructure materials, LMs gain additional improved properties. Nickel (Ni)[21,50,51] and Cu[19,52,53] offer semi-liquid properties, while gadolinium (Gd),[42] Ni,[43] and Fe[54] provide magnetic properties; CNTs[22] provide mechanical strength, while Au[44] and Ag[45] can be used to improve the conductivity of the LMNCs. The semi-LM is a nanocomposite that is between a liquid and solid, *i.e.* similar to a paste.

Additionally, mixing with nanomaterials can offset some limitations of the LM in certain applications. For instance, LM has high surface tension and it is difficult to maintain the shape; however, when mixed with silicon elastomers to create LM silicon ink, the printed shape can be retained. The electrochemical patterning method, where the electrodes determine the pattern of the LM, was successfully demonstrated for geometrically shaped electrodes (*i.e.* triangle, square, and circle) in 3D printers.[55]

LMNP-based materials

LMNPs were first prepared by dispersing EGaIn in ethanol using a homogeniser. Then, films were prepared by casting/spraying LMNPs. As volatilisation of the solvent behaves as an insulator, the oxide layers on the LMNPs should be broken to improve their electrical conductivity and ability to combine with other nanoparticles,[56] since the dispersed nanoparticles were covered with oxide layer that is formed under exposure to oxygen in result of natural adoption of core–shell structure.[1] Even though the resulting oxides can hold the original LM shape, which is good for 3D printing, they are not suitable for reconfigurable electronics.[57] Here is a small discussion about oxide layer in addition to mentioned above. It has been demonstrated that the application of heat to LM microparticles ruptures the oxide layer, which in turn leads to phase segregation as a result of thermal expansion and surface oxidation. Changes in surface roughness and composition and oxidation have also been observed. Because it is performed at high temperatures, thermal sintering produces a very thick surface oxide layer that prevents further oxygen penetration and the coalescing of particles beneath it.[58] Increasing the temperature enables further oxidation, and thermogravimetric analysis (TGA) results have shown that a new oxide layer will form on top of a smooth passivating layer of Ga LM at a temperature of 773 K. New layers such as these will exhibit some variations in surface texture as a result of a potential thermal gradient and proximity to the pan walls of the TGA device. The thick oxide shell can also induce surface cracking at points of high curvature.[59] The destruction and coalescence of the nanoparticles is called sintering, which is achieved by mechanical pressure application,[53] inkjet printing,[60] laser printing,[58,61,62] heating,[58] and evaporation.[63] This mechanical pressure can be applied *via* manually patterning[53] or by placing the LM in a microchannel.[64] In writing applications, LMNP films are patterned directly using a knife[60] or marker[64] and then sealed with PDMS. Although the width of the writing line will vary depending on the thickness of the tip of the knife or marker, it is possible to create any shape using this method. To apply the microchannel method, LMNPs are dispersed and poured into microchannels using a syringe (Fig. 2a) and then pressurised over the PDMS. This method is more accurate than hand-drawing and produces an electrically conductive area that can

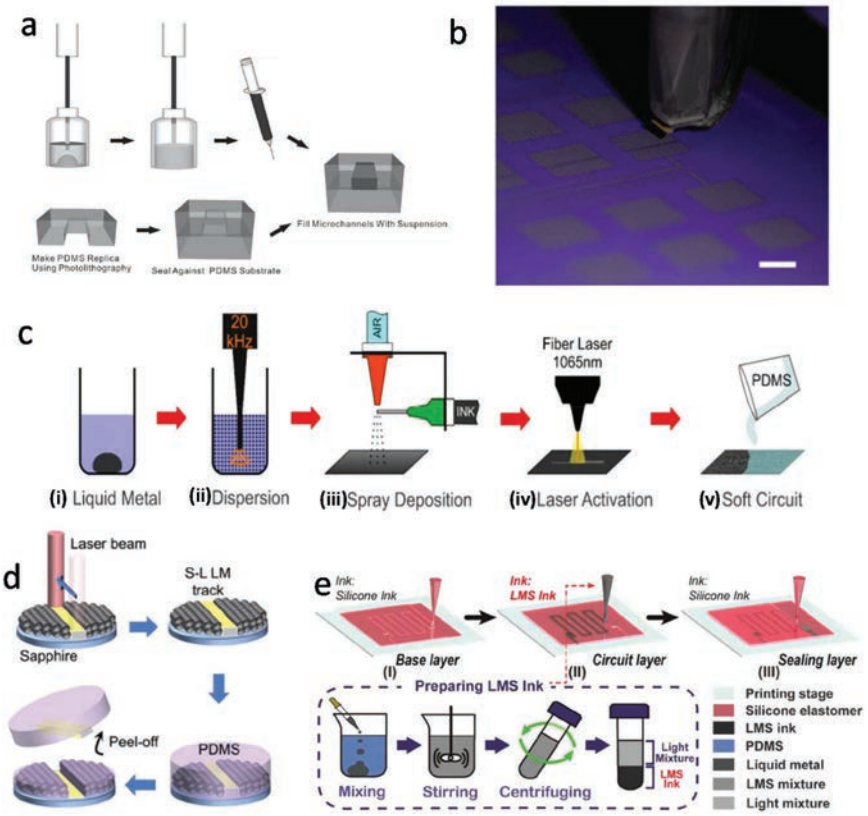

Fig. 2 Patterning methodologies: (a) fabrication of microchannels through encapsulation of LMNPs;[64] (b) LMNP patterning *via* inkjet printing;[60] (c) LMNP patterning *via* laser printing;[61] (d) transferring laser-printed LMNP patterns on Si wafer substrate onto PDMS substrate;[62] (e) process for producing LMS patterns and ink.[66]

be selected afterwards, allowing the thickness and microfluidic substrate to be tuned to vary the critical pressure of mechanical sintering. The resolution of a trace can be improved by injecting particles into microfluidic devices.[64] Inkjet printing is an advanced method for mechanically applying pressure that enables the precise patterning of conductive material onto substrate. Thiols can be added to the LMNP dispersion solvent to reduce the surface tension for fine inkjet patterning. A 1 μm layer of LMNPs can be sintered and patterned through inkjet injection (Fig. 2b).[60] Stretchable circuits based on EGaIn-NP ink can be patterned by applying inkjet printing to a PVA substrate with 20 μm-thick conductive lines.[65] In laser sintering, a laser is used to heat the ink, causing the nanoparticles to expand, rupture, and coalesce;[58] using a slightly different mechanism, dispersion can be achieved through mixing with thiols. Irradiating an LM with a laser causes it to thermally expand and then shrink, which in turn causes it to rupture and leak. When LMNPs are heated to above their vapor point, the thin oxide shell cannot be restrained from vapourising, and vapour will radiate from the metal core. The LMNPs will then cool in the air and form metal oxide nanoparticle assemblies comprising nanoparticles attached to a substrate, which can act as a seed layer to promote the wetting of unvapourised LM.[62] When the oxide nanoparticles and core coalesce, a pattern will form;[62] deformations such as these are more pronounced at higher laser powers. In pulsed laser sintering in particular, the precision and fineness of the patterning will depend on the laser spot diameter. Pulsed laser sintering is often more accurate than other methods, as the laser diameter can be as small as 37 μm, which provides a resolution and patterning precision compatible with small and high-density soft electronics.[61] Following laser sintering and prior to encapsulation, LM can be spray-printed and patterned onto the PDMS substrate[58] (Fig. 2c), enabling the removal of unnecessary LMNPs from the PDMS *via* ultrasonic cleaning.[62] Silicon wafers are also sometimes used as the substrate. In this case, the pattern can be transferred to the PDMS by casting and peeling off the PDMS (Fig. 2d).[62] In the heating method, the dispersed LMNPs are sprayed onto the PDMS patterned on a ceramic substrate using a laser machine, and the PDMS mask is peeled off and sintered *via* heating.[58] Flexible substrates cannot be used because of the very high temperatures (300 °C to 900 °C) used for sintering. The sintering mechanism is also different from that of the laser method; the surfaces of the LMNPs are deformed when temperature is applied. As the temperature increases, it accumulates on the surface of the inner liquid part, causing further partial rupturing. At higher temperatures, the momentum of the rupture increases, and nanowires are generated on the surfaces of the LMNPs. The interconnections of these nanowires then provide conduc-

tivity.[58] Therefore, the resistance of sintering is higher than that of the laser. In the evaporation method, the dispersed particles are deposited on the substrate by mask printing, channel deposition, handwriting, or drop casting and dried for at least one day under ambient temperature and atmospheric pressure. Skin, plant leaves, glass, and PDMS can be used as the substrates, and the dispersed liquid is different from that in the other methods. A solution of biological nanofibrils (NFs), such as cellulose, silk fibroin, and amyloid, dispersed in pure water is used for dispersion of the LMNPs. The biological NFs reduce the size of the LMNPs and increase their stability during dispersion. Since the film is then separated on NF-rich and EGaIn-rich layers after sintering, the resulting film has flexible conductivity and electromagnetic shielding properties, and its operating behaviour is responsive to humidity, light, and voltage.[63]

Semi-LM paste

Unlike ordinary LMs, semi-LM paste can utilise the specific properties of additive elements with high adhesion that can be easily attached to the surface. Two primary methods are used to fabricate LM paste: inducing intermetallic wetting between the LM and other metal particles in an acidic solution, and wetting the particles using the LM's sticky oxide under mechanical stirring.[67] To eliminate the oxide layer, a NaOH alkaline solution is used as a Cu–LM paste dispersion solvent.[19] A mechanical stirring method must be used to produce the Ni-LM paste[21] because a NaOH solution will not dissolve nickel oxides.[67] LM pastes have been successfully produced using Ni,[21,50,51] Cu,[19,52,53] and magnetic additives.[46] Printing techniques including stencil,[50] direct,[51] roller,[50] and transfer printing can be used to pattern semi-LM pastes. To carry out stencil and roller printing, Ni LM pastes are prepared by placing EGaIn and Ni particles into a glass container and mixing them using a glass rod, inducing deposition of the LM oxide film around the Ni particles. As the percentage of Ni particles increases, the adhesion strength increases and the conductivity decreases.[21] Stencils can be patterned onto silicone elastomer substrates by placing a metal mask onto the substrate and then rolling the Ni-LM paste over it (Fig. 3a) prior to sealing with a silicone elastomer. Using this approach, multilayered structures can be easily created.[21] Roller printing involves patterning directly onto a surface by utilising the difference between the surface adhesions of Ni-LM paste and polymethacrylate (PMA). Patterns are first projected using a projector and transferred using a ballpoint pen filled with PMA glue; a roller coated with Ni LM paste is then rolled on the surface (Fig. 3b) and, finally, the paste is sealed with an aqueous polyvinyl pyrrolidone coating.[50] In direct printing,[51] the Ni-LM paste is prepared by mixing Ni particles with galinstan in a vial using a homogeniser while the vial is cooled with water. When the percentage of Ni particles increases in this mixture, the modulus of elasticity, yield stress, and viscosity also increase. This change is more pronounced for nanoparticles than microparticles. In the case of 10 wt% of nanoparticles, immediate hardening is observed upon fabrication. The proportion of Ni particle mixing achieved with a homogeniser is less than that achieved by mixing with a glass rod. However, because of strong mixing using the homogeniser, it is possible to formulate a paste with a small weight percentage. A 3D printer is then used to directly print the pattern because the paste is more uniformly mixed than in that created by mixing with glass rods and the paste dispensing is stable. It is thus possible to print 2D as well as 3D shapes, and

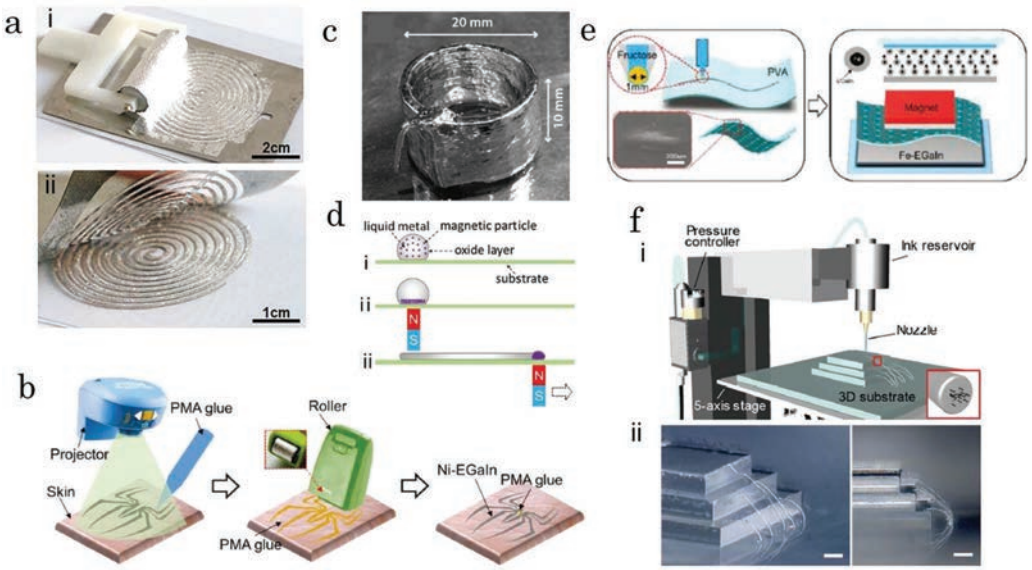

Fig. 3 Method of patterning semi-liquid metal: (a) pictures depicting (i) printing of Ni LM paste on an Ecoflex substrate by stencil printing with rolls and (ii) mask removal;[21] (b) procedure for roller printing of Ni LM paste;[50] (c) 3D-printed Ni LM paste structure;[51] (d) procedure for printing magnetic LM;[43] (e) procedure for fabricating LM pattern on a PVA substrate using the difference in surface adhesion;[54] (f) (i) 5-axis 3D printer for direct printing of CNT/LM composites, and (ii) stereoscopic micrograph of a CNT/LM composite printed on a stepped structure. Scale bar: 100 μm.[22]

the printed shape is not deformed by its own weight (Fig. 3c). When Cu particles were mixed with the LM, a paste was formed that was similar to that with the Ni particles[19,52,53] The Cu LM pastes were prepared by two different methods. In the first method, EGaIn and the Cu particles were weighed in a beaker and stirred into NaOH solution. After stirring, the NaOH was evaporated, and Cu LM paste was obtained.[52,53] In the second method, EGaIn and Cu particles were weighed into a Petri dish, and the oxide film was removed by applying a voltage to the NaOH solution. After this treatment, the NaOH solution was dried in vacuum to produce Cu LM paste.[19] Both these pastes were almost solid at a mixing ratio of 20 wt%. In the subsequent printing methods, 15–20 wt% was used because of ease of handling when the paste is closer to solid consistency. Two patterning methods were used with the Cu LM paste: roller printing[52] and transfer printing.[53] In roller printing, silk fabric is used as the substrate; first, a mask is placed on the fabric and polyvinyl acetate (PVAC) glue is screen printed on it. A roller is then used to print the Cu LM paste, which is selectively applied only over the PVAC glue as the adhesion of the paste is different between the fabric and the PVAC glue. The glue enables the Cu LM paste to adhere to a specific shape on the fabric as the glue expands and contracts. A silicone elastomer is then used to seal the printing. In transfer printing, coated papers are used as the printing substrates; the patterns are first printed on the coated paper using a laser printer, and the Cu LM paste is applied with a brush so that the paste only adheres over the toner. Next, the 3D-shaped silicone elastomer transfer substrate is prepared and pressed onto the printed substrate such that the Cu LM paste transfers to the elastomer. After transferring the paste, the printed pattern is sealed with a thin layer of silicone elastomer. LM paste can also be produced by mixing LM with quartz to form a paste similar to Ni- and Cu-particle pastes.[67] Unlike Ni-LM and Cu-LM pastes, however, quartz LM pastes can be separated into their LM and quartz constituents by stirring in an acidic or alkaline solution. Quartz-LMs can be produced by stirring while the LM oxide layer forms, and separated by stirring in an LM oxide-layer-dissolving solution. By adding or removing quartz powder in this manner, the rheological characteristics of the paste can be reversed. Unlike other LM pastes, which only have high conductivities, quartz-LM pastes also have good adhesion properties.[67] Two methods are commonly used to prepare quartz LM pastes.[67] The first involves stirring with a glass rod in a beaker, and the second involves stirring in a ball mill machine. The latter method allows more uniform mixing and finer crushing of the quartz particles. Patterning is achieved by stencil printing on a fabric substrate. A stencil mask is placed on the fabric and the quartz LM paste is applied with a brush; the pattern is then obtained by removing the mask. The adhesion mechanism of quartz LM paste is as follows. When the quartz LM paste is in contact with the substrate, shear motions cause small droplets to be pushed out through the gaps between the particles; these droplets form a new oxide/substrate interface and enable strong adhesion.[67] LMs can achieve magnetism when mixed with magnetic metal particles[42,43,54] to enable magnetic patterning. Gd,[42] Ni,[43] and Fe[54] have been reported as examples of available metals with magnetic properties. The use of magnets for patterning simplifies the printing process and allows printing on superhydrophobic substrates, printing in closed spaces,[43] and repairing damage after encapsulation.[54] The preparation of magnetic LM (MLM) ink begins with the mixing of Gd with GaIn and Ni with EGaIn, with a mortar and pestle used to break the Ni and Gd particles down to several micrometres and nanometres in diameter, respectively.[43] Micrometre-scale Fe particles are then mixed with the EGaIn using a glass rod.[54] The mixing ratio can range from a few percent by weight upward; increasing the ratio produces an MLM with enhanced magnetic properties very similar to those of a magnetic metal[42] and increases the conductivity, ink line width, and droplet volume.[43] However, increasing the mixing ratio also causes the droplets to become less fluid and prone to separation from each other.[54] Ni and Fe MLM inks for which simple bar magnets[54] can be used for patterning have been demonstrated. Substrates for Ni and Fe MLMs can be made from paper, PDMS, a hydrogel, eggshells, or glass, and MLM ink can be printed onto a substrate by moving a magnet underneath it (Fig. 3d). Using this method, it is also possible to print onto the inner walls of a microtube by injecting MLM ink into the microtube and then moving a magnet located outside of the tube to create the printed pattern. MLM can also be transferred to a thermoresponsive hydrogel that can be polymerised within the microtube following the printing process. Following dehydration by heat, the hydrogel can be detached from the microtube, carrying with it an MLM ink that will adhere to the hydrogel even after absorbing water. It is also possible to print onto two surfaces with different adhesive properties[54] using polyvinyl alcohol (PVA) film as a substrate and fructose, which has a higher degree of adhesion to MLM ink than PVA film, as the adhesive agent. By forming the PVA on a glass plate, a film with a flat and smooth surface and projections limited to several tens of micrometres in size and distributed at equal intervals can be obtained. The protruding surfaces serve to protect the ink-applied surface when the film is stacked. Fructose is patterned on the smooth surface of the PVA film using a ballpoint pen and a mechanical control arm. A magnet is placed on the PVA film over a container of MLM ink, which is then attracted to the PVA surface. As a result of the difference in adhesion between the PVA and fructose, the MLM ink adheres only to the fructose (Fig. 3e). A multi-layered structure can be constructed by interconnecting the layers with holes. It is also possible to transfer such patterns using heat, as the hydrogen bonds between the LM oxide and fructose layers can be broken at elevated temperatures (*e.g.*, 80 °C). By attaching PVA films printed with MLM ink to silicone elastomer substrates, their patterns can be transferred by heating to 80 °C, enabling the transfer of patterns with very little loss. The formation of 3D shapes is easier when CNTs are mixed with the LMs; CNTs increase the mechanical strength of the LM and allow 3D printing in various dimensions. The method for preparing CNT/LM composites is as follows. First, CNTs are treated with 70% nitric acid to form a small number

of carboxyl groups on the walls of the nanotubes. Carbon impurities and metal catalysts used in the synthesis of CNTs are thus removed by acid treatment. The treated CNTs and Pt are next dispersed in pure water, and the walls of the CNTs are coated with Pt by static electricity. The Pt-CNTs generated thus and EGaIn are dispersed separately in 1-methyl-2-pyrrolidone (NMP) by ultrasonication. They are mixed and continuously stirred in an N_2 atmosphere until the NMP evaporates completely. The interfacial material Pt helps the CNTs to uniformly disperse in the LM. Because the contact angle of the Pt is smaller than those of other metals, Pt has high affinity for LMs. The fabricated CNT/LM composites are subsequently printed directly using a 5-axis 3D printer (Fig. 3f-i). Therefore, CNT/LM composites can be used for bridge wiring and printed on structures that have steps and gaps (Fig. 3f-ii). This type of wiring has a higher resolution (minimum diameter of 5 μm) than wires obtained by commercial wire bonding techniques; in addition, it shows high electrical conductivity equivalent to that of conventional metal wiring.[22]

LMNCs

Some of additive materials of LMNCs are briefly summarised herein. A method for fabricating nanosized film patterns using thermal evaporation has been reported. Herein, a polyimide film mask is placed on a silicone elastomer substrate, such as PDMS, and Au is sputtered onto it. Ga is then thermally deposited on this substrate, and the required pattern is obtained by removing the mask. In addition to polyimide film masks, photoresist masks can be used. With a photoresist mask, a line width of 10 μm can be printed; Ga thus accumulates on the surface when its ratio is higher than that of Au (atomic ratio greater than 3.9).[44]

Another reported method for coating LM following Ag paste inkjet printing involves the use of tattoo paper as a printed substrate, which enables the pattern to be transferred to various shapes and surfaces. In addition, since the Ag nanopaste and LM are applied separately, there is no need for complex ink production and printing. First, the Ag nanopaste is printed on tattoo paper with a commercial inkjet printer; EGaIn is then dropped onto the pattern and rubbed over the printed area using a cotton swab. A 2% solution of acetic acid is applied for a few seconds to remove the excess EGaIn; the patterns are then washed with pure water and dried in an oven. The electrical properties are drastically improved in this case compared to those of the Ag nanopaste. This fabricated pattern shows 106 times higher conductivity and maintains low trace resistance when bent and stretched to 80% strain.[45] The LMNPs dispersed in silicone elastomers have been reported in the literature;[66] these are called LM–silicone (LMS) inks and are suitable for 3D printing processes involving direct ink deposition. The method for producing LMS ink, which is shown in Fig. 2e, involves adding LM to a silicone elastomer (PDMS) and then mixing the two *via* shearing to produce a mixture of particles and a silicone matrix. As the LM particles are dispersed in this mixture, good flowability and insulating properties can be achieved even at high volume fractions. Thus, it is impossible to print 3D shapes. Therefore, LMS ink was obtained by concentrating the LM particles by centrifugation; this ink has strong shear reducibility and can be easily pushed out of a fine nozzle. In addition, the high storage modulus and shear stress enable retention of the printed shape. The ink is directly deposited on the silicone elastomer substrate and then encapsulated. In this state, the ink is not yet conductive; after encapsulation, the material becomes electrically conductive upon activation by pressure or by freezing to −80 °C. These mechanisms are in the following order. For activation by applied pressure, the LM particles coalesce with each other. LMS ink has low electrical resistance and low hysteresis but wiring using this ink has high resistance to stretching; thus, it is easy to form a multilayer structure. The most important difference between ordinary LM wiring and LMS ink wiring is the resistance to damage. Owing to the high fluidity of ordinary LM wiring, the LM leaks out when damaged. However, the LMS ink does not leak when damaged; it can maintain its conductivity, and the change in resistance due to damage is within acceptable limits.[66]

Applications of LM-based nanocomposite materials

In the preceding section, techniques for fabricating and patterning LMNP and LMNC materials were discussed. In this section, the use of LMNPs and LMNCs in flexible electronics applications—with a focus on flexible sensors, actuators, and batteries—is discussed. In fabricating flexible electronics, heat-free mechanical soldering is useful because it enables the manufacture of sheet-like structures, the joining of undercooled LM particles through coalescence and solidification, the joining of thin metal films, and the healing of surface defects in thin films. Heat-free techniques can be used to sandwich undercooled particles with thin films (Au and Al), enabling the production of multiple joints using fewer or smaller particles through the tuning of applied stresses such as orthogonal stress.[35] In addition to enhancing the applicational performance of different types of devices, LM-based nanocomposite materials are beneficial for battery energy storage systems, in which LMNCs are often used as anodes because of their self-healing property, which boosts battery capacity and stability. LM-based nanocomposite materials alter the mechanical properties of sensors and the conductivities of actuators, enabling their application in the soft robotics used in drug delivery systems.

Sensors

LMs are widely used in several types of sensors, such as gait sensors,[72] wireless strain sensors,[73] pressure sensors,[74] and optical sensors,[75] because of their high elasticity and high level of biocompatibility. Since LM has high rigidity against deformation, they have been mainly used in sensors requiring high elasticities. In recent years, sensors that realise more functions in combination with LM and other nanoparticles

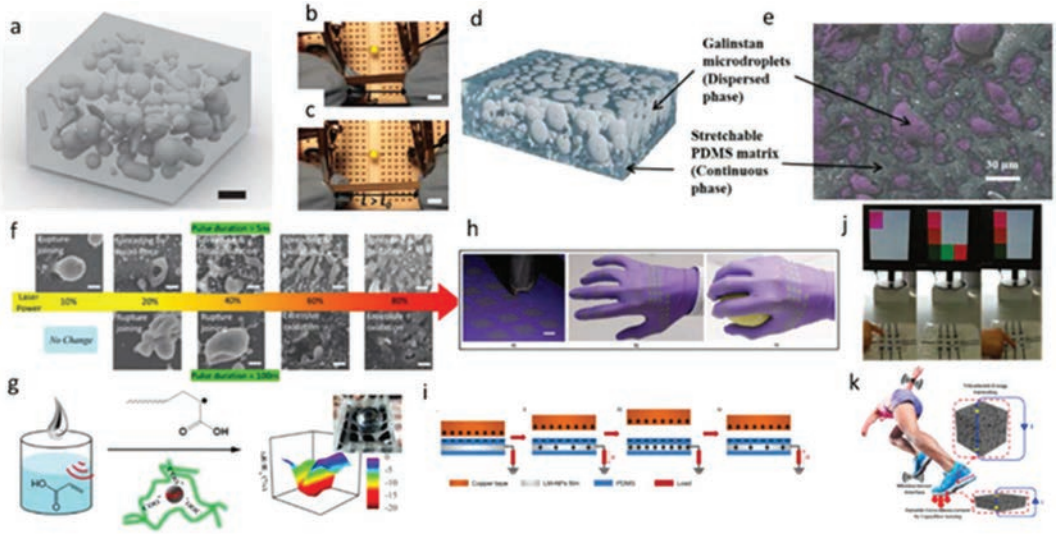

Fig. 4 (a) Illustration of composite (scale bar = 25 μm).[68] (b and c) LED circuit unaffected by strain.[68] (d) Material schematic of LM-PDMS composite,[69] and (e) scanning electron microscope (SEM) image showing dispersion of LM droplets (pink colour) inside a flexible and stretchable PDMS matrix (scale bar = 30 μm).[69] (f) Evolution of LMNP morphology as the laser power increases from 10 to 80%. The laser power is normalised against a 100% pulse fluence of 20 mJ cm^{-2}. The two cases shown occur at pulse durations of 5 and 100 ns, respectively; scale bar: 200 nm.[62] (g) Graphical depiction of the fabrication and application of a hydrogel-LMNP composite device.[23] (h) Inkjet printing of EGaIn nanoparticles onto a rubber glove for use in stretchable electronics.[60] (i) Working mechanism of the LMNP-based triboelectric nanogenerator.[70] (j) Application of 3 × 3 tactile interfaces as trigger keyboards.[70] (k) Concept of smart footwear with energy harvesting, force sensing, and wireless data connectivity capabilities.[71]

have been proposed. Herein, LM particle usage in sensors is discussed under three broad categories: (1) using LMNPs with elastic insulation materials, (2) using LM with rigid metal nanoparticles, and (3) using other nanoparticles aside from LM to obtain new characteristics *via* interactions.

Sensing system using LMNPs. Since LMs have excellent electrical properties, studies have been conducted to evaluate their electrical properties when mixed with materials having poor conductivities. A method to endow electrical properties on highly elastic polymers by dispersing LMNPs into the polymer has been proposed[68] (Fig. 4a–c). It is impossible to obtain good conductivity by only adding LM inside the nonconductive polymers. However, this study succeeded in obtaining conductivity selectively by applying concentrated pressure, under which the LM distribution in the polymer changed and the particles were partially interconnected. Thus, an arbitrary circuit was formed on a polymer and LM composite, and the resulting wiring behaved as a strain sensor.

A pressure sensor was fabricated by dispersing LM particles in PDMS[69] (Fig. 4d and e). Conventional LM pressure sensors are based on piezoresistive effects of the LM wiring; such sensors indicate the change in resistance based on the applied pressure. Currently, this sensor conducts only when a certain pressure is applied. In addition, the threshold pressure can be adjusted according to the amount of LM to be added.

It has also been reported that a similar effect can be obtained by laser irradiation rather than by applying physical pressure[62] (Fig. 4f); research shows that it is possible to obtain an LM with a two-phase structure where the LM and solid oxide phases are separated by irradiating the LMNPs with a laser. Arbitrary wiring has been successfully achieved using this method, and the obtained structure can be used as a strain sensor and microheater.

It is generally known that ultrasonication of a LM in a solvent produces fine nanoparticles,[16,31,64] and a study has reported the fabrication of stretchable strain sensors using this technique[23] (Fig. 4g). In the study, LM particles were dispersed in a hydrogel by ultrasonication, and gelatinised LM particles were wired as strain sensors. The device thus behaved as a robust composite by combining the ions in the gel with Ga ions to constitute a core–shell structure. This device not only has high elasticity and good electrical characteristics but is also self-healing.

Another study[60] reported a sensor, electrode, and wiring that was integrally moulded on a rubber glove (Fig. 4h). This highly elastic conductive material was prepared by printing LMNPs directly using an inkjet printer; the LMNPs were fabricated by ultrasonication and thiol self-assembly, and the average particle size was tuneable in the range of 180 nm to 600 nm. Similarly, power generation using a nanocomposite sheet containing nanoparticles dispersed by ultrasonic treatment has been reported[70] (Fig. 4i and j); herein, LMNPs were patterned on a PDMS film, and power was generated by triboelectric charging using a copper foil. Thus, a pressure sensor that allows measurement of the applied pressure using current is achieved.

A method of manufacturing a triboelectric power generation device and a capacitive sensor using LM particles and soft silicone elastomer has been proposed[71] (Fig. 4k); this sensor is fabricated by mixing LM particles with the silicone

elastomer and moulding them into a porous structure using salt. The developed sensor can detect pressure through capacitance changes due to deformation based on the applied pressure, thereby harvesting electrical power from motion through a smart device embedded within the user's shoes.

LM with addition of other nanoparticles. In recent years, numerous studies have been conducted on changing the characteristics of LM by the addition of metallic or non-metallic particles. It is possible to change the electrical, mechanical, and magnetic properties by adding other materials into the LM, and the physical properties can be varied according to requirement. The mixing of fine copper particles into LM was proposed[19] (Fig. 5a) for improving the electrical and thermal conductivities. This work shows that certain characteristics can be obtained by alloying Ga-based LM with copper particles and that the mechanical characteristic of this material can be changed by the amount of copper particles added. Through this work, the LM is shown to have behaviours similar to a solid–liquid two phase material, which allows excellent workability for the LMNCs, that is better than for pure LM. This technique was also applied to study Ni particles mixed in LM[76] (Fig. 5b and c). Mixing Ni particles into an alloy of Ga and In produces a gum-like material with high electrical conductivity and good adhesion. Hence, it can be directly printed on substrates made of various materials as well as used for the fabrication of highly stretchable sensors. A data glove using such a sensor was demonstrated to be able to read finger actions, indicating its suitability for wearable devices. However, there have been reports of alterations in the mechanical properties of LMs through mixing with CNTs[22] (Fig. 5d). In the study in question, the physical connections between the LM particles were enhanced by adding fine Pt particles and CNTs to improve the mechanical strength of the LM. Using this nanocomposite material, three-dimensional wiring with LM is enabled with high elasticity, and the change in electric resistance due to deformation can be measured.

In addition to such physical sensors, sensor applications for detecting magnetic forces have been proposed. Magnetic fluids are widely used in liquid-state magnetic applications owing to their unique magnetic and fluid characteristics;[77,78] however, in recent years, many magnetic devices using LM have been proposed because of their high boiling points and low volatilities. In order to provide magnetic characteristics to LM, several studies have reported the dispersion of Fe and Ni particles in LM.[79–82] Metallic glass composed of Fe [73.5]: niobium (Nb) [3]: Cu [1]: silicon (Si) [13.5]: boron (B) [9] has been mechanically mixed with two kinds of LM (Fig. 5e–h), namely gallium–tin (Ga–Sn) and Ga–In, to produce magnetic LM with strong magnetic forces and sensing capabilities with respect to temperature.[83]

Interactions between LM and other particles to obtain new characteristics. To sufficiently utilise the functionality of LM, several methods have been proposed to not only fabricate LMNPs or disperse other material particles in LM but also use nanomaterial composites in the peripheral environment of LM. In the past, several studies were conducted to fabricate highly stretchable physical sensors by filling LM into channels formed on flexible silicone elastomers.[84,85] A highly stretchable sensor capable of detecting magnetic fields in addition to physical forces was fabricated and reported[86] (Fig. 6a and b). This sensor detects tension and pressure *via* the electrical resistance of the LM wire, which changes according to the applied physical force. In addition, Fe nanoparticles are dispersed in the elastomer constituting the flow channel, whose flow path diameter is changed by the applied magnetic field.

LM sensors and wiring using Ga-based films with liquid–solid two-phase structures have been reported[44] (Fig. 6c and d); in the study, Ga and Au are alloyed on an Au surface by thermal vapor deposition, and the alloy was fabricated on a PDMS thin-film substrate. Vapor deposition of Ga on an Au film produces a two-phase structure in which the liquid Ga and solid Ga–Au alloy are mixed. This solid–liquid two-phase

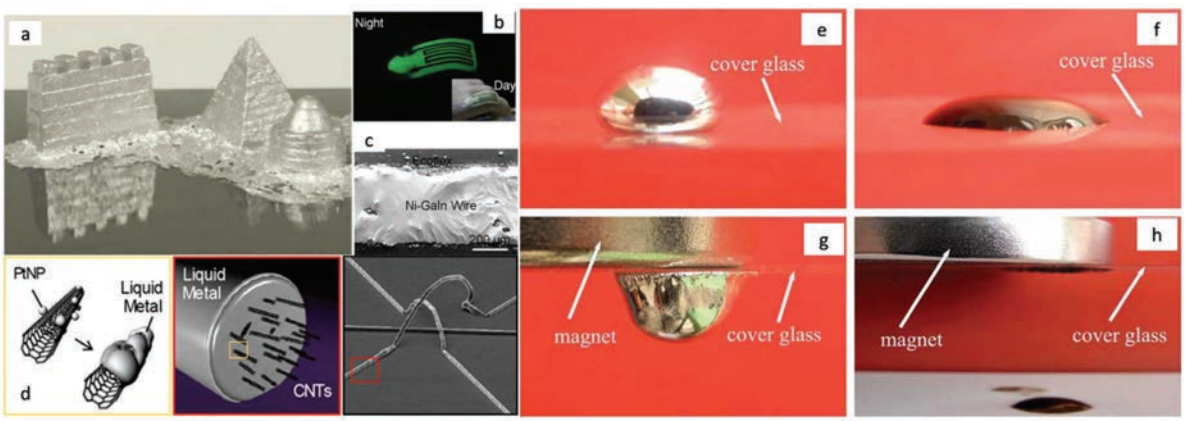

Fig. 5 (a) Free-standing TransM2ix "sandcastles" made by moulding (left: ϕ = 0.15; middle and right: ϕ = 0.20); scale bar: 10 mm.[19] (b) Luminescent behaviour of the wearable Ni–GaIn sensor on the finger;[76] (c) surface SEM image of the directly printed Ni–GaIn wire on an Ecoflex substrate;[76] (d) schematic illustration showing the preparation of the CNT/LM composite using Pt as the interface material, and an SEM image of the 3D printed CNT/LM composite;[22] (e and g) behaviours of the droplets of Ga [85.8]: In [14.2] magnetic functional fluid and (f and h) water-based fluid.[83]

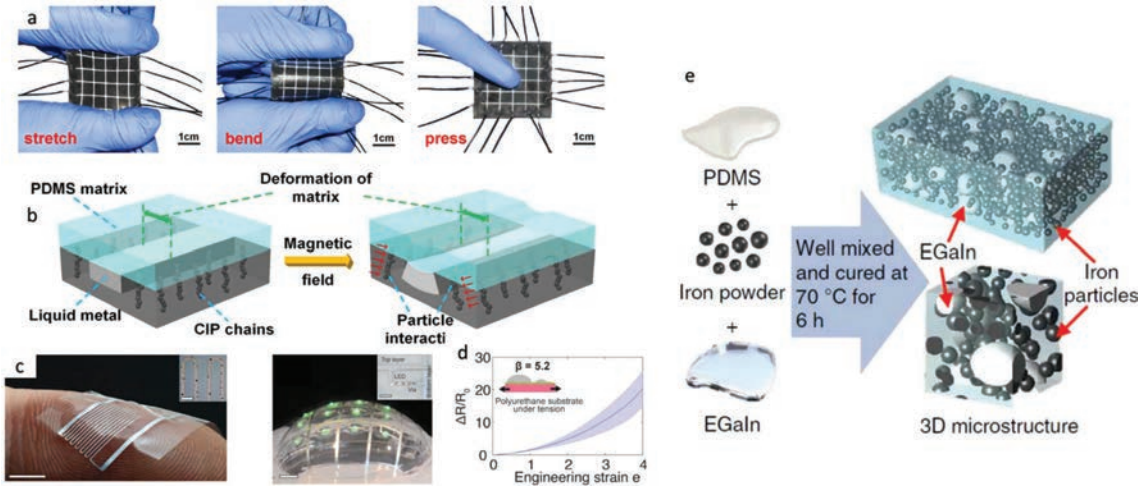

Fig. 6 (a) Digital images of the LM based magnetoresistive strain sensor (LME-MRE) array under various types of mechanical deformation;[86] (b) schematic illustration of the magnetic–electric coupling sensing mechanism;[86] (c) stretchable biphasic (solid–liquid) thin metal films for flexible electronics;[44] (d) relative changes in the electrical resistance of a biphasic Au–Ga conductor prepared with an atomic ratio of β = 13 and deposited on a polyurethane substrate (n = 10 samples, ±S.D.);[44] (e) schematic of the procedure for fabricating the LM-filled magnetorheological elastomer.[87]

metal wire showed electric resistance changes to deformation without breaking under large deformations. In the study, an application to detect the bending of the finger was demonstrated. A strain sensor with a positive piezoresistive effect was fabricated by dispersing LM particles with other metal particles in a silicone elastomer[87] (Fig. 6e). The resistance of a conventional piezoresistive sensor increases with tensile deformation, but the resistance of the proposed sensor decreased during stretching. Furthermore, owing to the acquired characteristics from the added metal particles, the sensor could detect magnetic fields.

Actuators

The wide range of applications of wearable devices and soft robots suggests that stretchable electronics have great potential in the future. The most important characteristic of stretchable electronics is their ability to maintain reliable and stable performance under mechanical deformation.[88] With the rapid development of technology, it is important to maintain good conductivity while withstanding large strains.[89] For a stretchable device, stretchability and good conductivity are important attributes; hence, it is a challenge for many researchers to develop such devices by selecting suitable materials with the desired properties (high stretchability limit and stable conductivity). Herein, we briefly discuss the conductivities of LMNCs and LM-based soft robotic materials in transportation systems.

In recent years, with the rapid development of wearable electronics and soft robots using stretchable actuators, stretchable technologies have become an important emerging field, and innovative research on the application of actuators to sensors and circuits has gradually developed from the potential of materials to stretch like rubber.[90] LM wires can be stretched to a greater length than conventional wires, and the LMs not only have low Young's moduli but also retain excellent conductivities under large deformations; therefore, Ga-based LM is used in stretchable circuits. Depending on the composition of the LM, there are different methods to manufacture stretchable electronics. The LM has very good fluidity and is softer under tension than the commonly used materials for stretchable electronics. Using this property to inject LMs into stretchable channels is a simple and convenient method of fabricating stretchable devices. For example, when LM is injected into hollow poly(styrene-*b*-(ethylene-*co*-butylene)-*b*-styrene) fibres, the resulting stretchable conductors can maintain good conductivity even at 700% deformation.[91] This method can be used to develop complex and scalable conductors for sensitive pressure sensors; for example, by injecting an LM into a channel with a Wheatstone bridge structure, the sensor can detect pressure changes below 50 Pa with response times as short as 90 ms.[74] A lead wire can be fabricated by injecting LM into a spring-like spiral, stretchable channel. When the lead wire is stretched, a resistance changes of only 1/100th of that of the normal LM lead wire is produced, so actuators can be more stably controlled by using them as heaters.[24]

LMs have excellent thermal conductivities; thus, their uses for cooling have been considered. With the development of wearable devices and soft robots in recent years, improving the speed of heat conduction has also become an issue. Composites in which LM particles are dispersed in a platinum (Pt)-catalysed organosilicon elastomer have been developed (*e.g.* Ecoflex 00-30) with a low Young's modulus (<100 kPa), high deformation limit (>600%), and high conductivity[47] (Fig. 7a). This material can rapidly dissipate heat without allowing the production of electricity *via* high-strength and repeated expansions and contractions. With the advent of newer electronics and the 5G age, electromagnetic interference (EMI) is one of the problems that must be addressed. 3D LM-

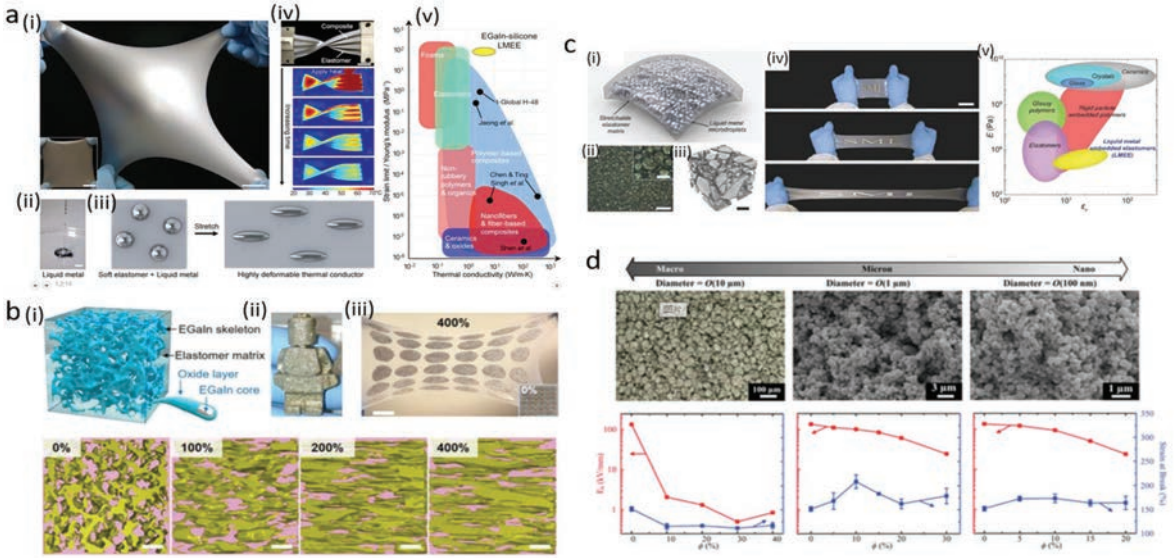

Fig. 7 (a) Thermal conductivity of the LM with soft composite,[47] (b) strain test of LM with soft composite,[92] (c) stretchable dielectric based LMEE,[93] (d) LM-elastomer nanocomposites.[8]

skeleton-based polymer composites are stretchy materials that provide good conductivities, with up to 400% tension, while shielding large amounts of EMI[92] (Fig. 7b). Such materials have shown stable electrical conductivities and effective EMI shielding even after 10 000 cycles of tensile tests with up to 250% strain.

LM nanocomposites with polymer. LM droplets can be added to elastomers to produce systems with fully flexible electro-elastic properties[93] (Fig. 7c). The dielectric constants and maximum strains of LM-embedded elastomers (LMEEs) can be enhanced to more than 400 and 600%, respectively, of their non-embedded values. LM-elastomer nanocomposites with different sizes of LM particle have been compared in multiple experiments to study the effects of LM particle sizes on the dielectric and mechanical properties of composite materials[8] (Fig. 7d). When the LM particles are of the order of nanometres, the composite materials have enhanced electrical permittivities but do not have significantly reduced tensile and dielectric breakdown strengths. When the LM particles are of the micrometre order, the permittivity of the composite material improves, but the dielectric breakdown strength decreases considerably. This material property can be thermally controlled by embedded thermal actuators. A stretchable and reversible transitional insulator and conductor (TIC) with a polymer that can switch between the insulator and conductor *via* temperature changes has been reported[94] (Fig. 8a). At room temperature, the LM is surrounded by silicon resin, so that the LM particles are disconnected from each other and cannot conduct electricity. At low temperatures (T = 212 K), the LM solidifies and expands in volume, while the insulating polymer hardens and shrinks. In this state, the LM droplets in the TIC contact each other, causing large changes in the specific resistance. Because they can withstand up to 680% deformation, such switch-like properties strengthen the potential of the enabled TICs in microelectronic or soft robot applications. Generally, Ga-based LM is liquid at room temperature, but under low temperature environments, solidification occurs even when LMEEs are formed by embedding LM particles in the elastomers; thus, Ga-based LM products cannot be used in such conditions. Research on LMEEs and performance tests have been conducted by controlling the LM droplet diameters in composites and polymer materials[95] (Fig. 8b). During the tests, the LM droplets still retain good mechanical properties at low temperatures (<−80 °C) and operate normally. This finding extends the utility of LM composites in various fields, and conductors made of such materials maintain stable electrical conductivity and stretchability even in cold environments. LMEE actuators have been used in retractable wires of stretchable thermoelectric generators (TEGs) to collect electrical energy from the heat radiated by the human body in cold weather conditions[96] (Fig. 8c). Since the TEG is wrapped in the LMEE, it is soft and comfortable enough to be attached to the human body; further, it can serve as a heat sink, converting the collected thermal energy into electrical energy to drive sensors in other wearable devices.

LMNPs as conductors. The conversion of LMNPs into microfluids *via* mechanical sintering has been reported[64] (Fig. 9a). In this method, the LM is dispersed into nanosized droplets in ethanol by ultrasonication, and the resulting LMNPs are then transferred into PDMS *via* printing or injection. Finally, the insulating film of the LMNPs is broken through the application of mechanical pressure and connected to a stretchable lead wire with a specific shape. Systems for conducting this sintering process are easier to manufacture than laser sintering systems. A self-healing flexible composite based on LM microdroplets has also been reported[97] (Fig. 9b). This compo-

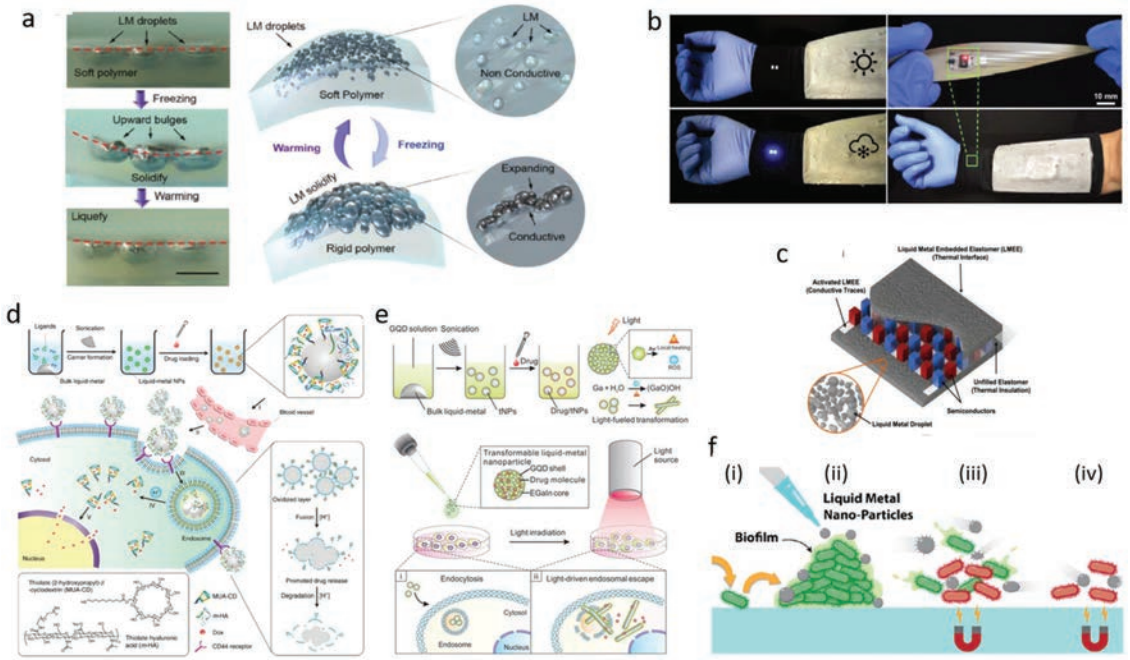

Fig. 8 (a) Phase change of LM nanodroplets,[94] (b) LMEEs at low temperatures,[95] (c) LMEEs integrated into TEGs,[96] (d) LMs in drug delivery systems,[99] (e) LM-based nanoscale transformer,[100] (f) MLM nanoparticles in antibiofilm activity.[101]

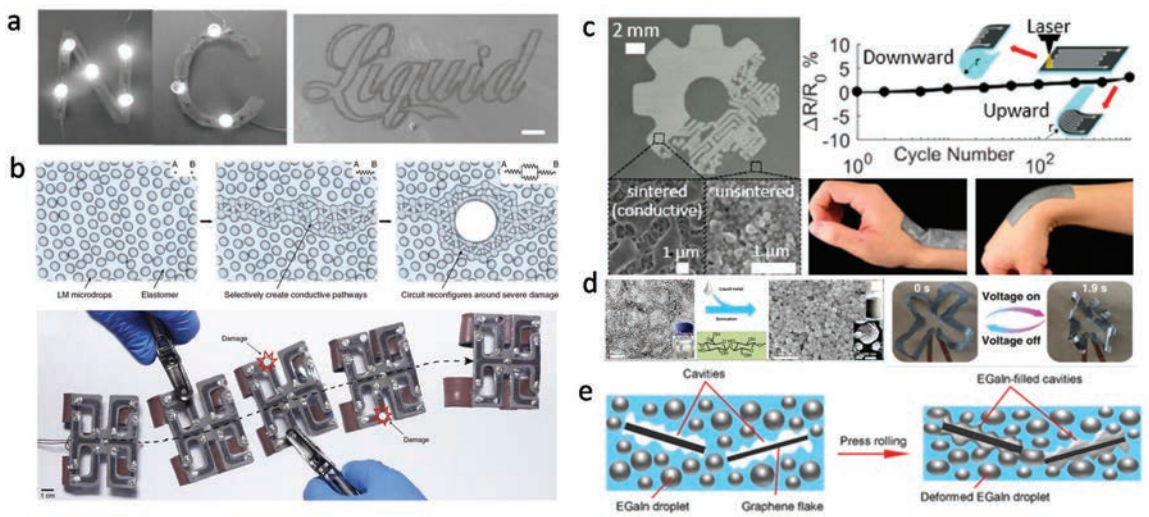

Fig. 9 (a) Microfluids with LMNPs;[64] (b) self-healing of LM nanodroplets;[97] (c) LMNPs produced by laser sintering;[61] (d) LM-coated nanofibrils and soft actuators;[63] (e) filling graphene flakes with LM.[98]

site material retains its insulating state upon inactivation and exhibits conductivity that does not change significantly upon deformation following activation. In the event of mechanical failure, the LM droplets around the failure point connect to their adjacent droplets to function as an electrical system. A soft robot developed with this material can continue to operate even when mechanically damaged. LMs form oxide films rapidly and have high surface tension but are incompatible with other materials; it is not easy to spontaneously composite LMs with other materials. Generally, electroconductivity is induced by mechanically squeezing the LM particles contained in the polymerisation species; however, this method reduces the integrity of the overall structure slightly. A stretchable device made of LMNPs can be rapidly produced by laser sintering[61] (Fig. 9c); by focusing and sintering with the laser beam, the oxide shells of the nonconducting LMNPs rupture, and the LM aggregates to form conductive paths. This method is highly accurate, fast, and mass-producible compared to con-

ventional physical sintering and can be used to fabricate multilayer soft electronic devices that are difficult to fabricate by conventional methods. Ga-LM based elastomers have good conductivities and large response limits, but their stretchability is susceptible to mechanical disruption, which affects conductivity. Biological nanofibrils (NFs) are used to induce LM droplets at ambient conditions for sintering the conductive coating layers to form composites with sufficient stretchability, conductivity, durability, and degradability[44] (Fig. 9d). It is believed that the sizes of LM droplets can be reduced by adhesion to NFs (>50 nm) and that approximately 0.05 wt% of NFs promote liquid bridge formation between the LM droplets during evaporative sintering. The various polar groups of the NFs enable excellent adhesion, expansion, and contraction of the LM droplets. A film composed of an EGaIn-rich lower layer and an NF-rich upper layer can be bent at high speeds (120° s^{-1}) in response to low voltage, light, and humidity; it is also an excellent material for a soft actuator. PDMS filled with LM and graphene shows high conductivity and stretchability as a composite material[98] (Fig. 9e). The graphene sheet fills with the LM when it is subjected to appropriate pressure and forms a conductive path even at relatively high pressures (>30 kPa), with minimal changes in the rate of change of electrical resistivity. This property renders compatible materials suitable for use as reliable lead wires under high pressure conditions.

LM in transportation systems. In addition to their excellent electrical conductivities, LMs have excellent performance in many applications, such as drug delivery (Fig. 8d). Delivering drugs safely to the designated area in the body maximises the therapeutic effects and has thus far been a difficult task. LMNPs with low toxicity are good candidates as drug carriers. An anticancer drug delivery system using LMNPs has been developed[99] (Fig. 8d); when LMNPs are fabricated using ultrasonic waves, the anticancer drugs are placed on the LM particles with functional groups that can distinguish tumours. Upon entry into tumour cells, the pH-responsive drugs are released, and the LM degrades. Although this method has not been observed to be toxic in studies, more assessments are needed before it can be used in humans. In later research, LMs were used to produce nanoscale transformers covered with graphene quantum dots (GQDs), which can deliver drugs efficiently[100] (Fig. 8e). In recent studies, low intensity rotating magnetic fields have been shown to control LM droplets to kill bacteria[101] (Fig. 8f).

Batteries: LM alloys for energy storage systems

Owing to their inherent deformability, high conductivity, and excellent electrochemical properties, LMs have been used in several applications as sensors and circuits,[102] with feasibility in the energy sector as well.[103,104] Among these, Ga-based and sodium–potassium (Na–K) alloys have attracted much attention in recent years. Since LMs that are made of these two alloys are in the liquid state at or near room temperature, they are free of thermal corrosion and sealing problems, with simple cell manufacturing processes compared to those for high-temperature LM batteries.[105,106] In addition, the problem of dendrite growth may be avoided by the self-healing function.[107] The role and future potential of LM in the energy sector are discussed in the remainder of this section, along with the latest research.

Ga and Na–K alloy-based active material. Ga metal and Ga-based alloys such as Ga–In have relatively low melting points and possess special electronic and thermal properties as well as fluidity.[108] Therefore, they are suitable not only for flexible and self-healing electronic components but also for batteries. Ga-based liquid alloys, which inherit the fluidity of LM, have the potential to avoid damage due to dendrites and volume expansion while maintaining high specific volumes as alloy electrodes. In an early study, the direct use of Ga as a Li-ion battery (LIB) anode was reported, with the capacity contributed by each stage of alloying yielding 91% of the theoretical capacity in electrochemical tests, as shown in Fig. 10a-i.[109] However, the cycling capacity of the cells in this study was limited to less than 30 cycles, and the capacity decreased to less than 500 mA h g^{-1} in the first 10 cycles. This indicates that extra thermal energy input is required and that cracks may occur in the intermediate stages, as shown in Fig. 10a-ii. Such large cracks can decrease the stability of the product.

In contrast, dual-element alloy electrodes, such as those made of Ga–Sn and Ga–In alloys, have melting points close to room temperature at eutectic concentrations, while ternary alloys like Ga–Sn–Li and Ga–In–Li have melting points above room temperature over the entire concentration range.[110,111] However, since these battery reactions are reversible, the alloy electrodes return to liquid phase and have the ability to recover from defects due to the high surface tension of the LM.

Chen's group reported Ga–Sn alloy particles dispersed in a framework of graphene oxide (GO) and CNTs as a self-healing LIB anode with excellent cyclability, capable of 4000 cycles at 4C (Fig. 10b).[112] Ga–In LM batteries that can achieve high cyclability without a complex framework for electrodes have been reported.[113] In these devices, bulk LM is dispersed into LMNPs using ultrasound waves and the resulting LMNPs are simply mixed with conductive carbon and binder before casting onto a current collector in the same manner as that used to prepare solid electrodes (Fig. 10c). Scanning electron microscopy was used to observe the LM droplets in the initial liquid state in the form of spheres, and absorption of Li ions turned the droplets into a nonspherical solid state; the delithiation process was used to restore the alloy to its spherical form. Compared with the bulk LM, the LMNPs are not pulverised or delaminated from the substrate, thereby confirming the stable and long cyclability. These studies show that no extra heating is required to obtain stable Ga-based self-healing LM anodes; the synthesis of LM into LMNPs eliminates volume expansion and provides a kinetic advantage, resulting in better cycling and kinetic performances.

While solidification of Ga-based LM electrodes can cause delamination and cracking, appropriate preparation of the particles dispersed in a conductive framework can effectively solve this problem. In addition, high-capacity anodes with excellent

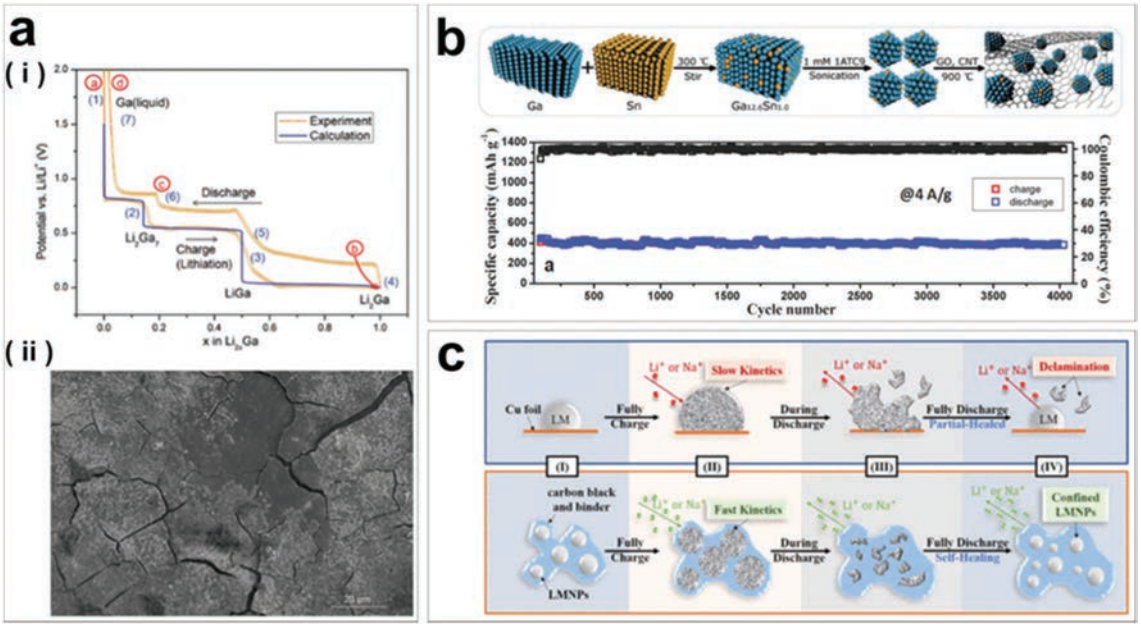

Fig. 10 (a) Ga-Based LM anodes: (i) cyclic voltammetry (CV) using Ga as an anode at 40 °C with cycling rate of 1C for self-healing, and (ii) the surface of the solidified Ga electrode after lithiation;[109] (b) Ga–Sn alloy with a CNT framework for an Li-ion anode;[112] (c) Ga–In alloy nanoparticles suspended in conductive carbon and a binder as LIB/SIB anodes.[113]

cycling characteristics can be developed as alternatives to the graphite and lithium titanium oxide ($Li_4Ti_5O_{12}$) used currently. Ga-LM-based flexible batteries have also been studied. The use of EGaIn as an anode material in the fabrication of a non-rechargeable cable-type battery (Fig. 12a)[114] has been demonstrated. The battery was shown to be highly flexible and elastic, with a bending radius of less than 1 mm and a stretchability of up to 100% strain. Furthermore, the battery could easily recover from any degree of bending without impairment of its electrochemical performance and exhibited a high degree of retention of its discharge performance after stretching. A self-healing conductor comprising Ni flakes, EGaIn particles, and carboxylated polyurethane incorporated in a robust energy storage device is fabricated (Fig. 12b);[115] this product is 200% stretchable without any performance degradation and retains its original capacity for 600 charging/discharging cycles and 1000 stretching/releasing cycles. A soft-matter, rechargeable, stretchable battery was fabricated with an EGaIn LM (eutectic alloy with 75 wt% Ga and 25 wt% In) anode, a manganese oxide (MnO_2) cathode, and an alkaline hydrogel electrolyte embedded in soft silicone packaging (Fig. 12c).[116] This battery could stably cycle within a voltage range of 1.40–1.86 V at 1 mA cm^{-2} while subject to 100% tensile strain.

Alkali metals (*e.g.* Li, Na, K) are promising anode materials owing to their high specific volumes and low redox potentials.[117–122] However, secondary batteries using alkali metals are prone to infinite volume changes during cycling, parasitic reactions with the electrolyte, dendrite growth problems leading to short circuits, and safety issues. Various approaches have been considered to solve these alkali metal problems, including preparation of new liquid electrolytes, development of solid electrolytes, design of artificial solid electrolyte interphases (SEIs), and adoption of nanostructured current collectors.[113,123–125] Although the alkali metal volume change and electrolyte problems during cycling have been significantly alleviated, the dendrite problem is specific to alkali metals and needs to be resolved. In this regard, LM anodes can be adopted as a promising strategy to mitigate dendrites in alkali metals.[126] In contrast to solid electrodes, liquid electrodes are deformable and self-healing;[127] in commercial Na–S and Zebra batteries, long-life and dendrite-free operations have been demonstrated using hot molten Na as the anode and solid electrolyte membranes as separators.[128] It has been reported that Na and K can form liquid alloys at room temperature and may be promising alternative anode materials in high-energy and safe alkaline ion batteries.[107,129]

The room-temperature LM Na–K alloy can be absorbed onto a porous carbon substrate to produce a high-capacity K-ion anode without dendrites (Fig. 11a).[107] Moreover, the Na–K anode can be applied to porous membranes such as carbon (C), Ni, Cu, and aluminium (Al) using the vacuum penetration technique (Fig. 11b).[130] The electrodes can be retained within the porous membrane even when they are bent or in contact with the separator. The designs for the Na–K–Al membrane anode, $Na_2/3Ni_1/3Mn_2/3O_2$ cathode, and common carbonate electrolyte containing sodium perchlorate ($NaClO_4$) for room-temperature rechargeable Na-ion batteries (SIBs) have been demonstrated. The LM Na–K anode coupled to a graphite-intercalation compound (GIC) is reported,[131] where a symmetric cell with the designed Na–K anodes exhibited unprecedented cycling stability at very high current densities (Fig. 11c). A novel dendrite-free self-healing potassium oxide

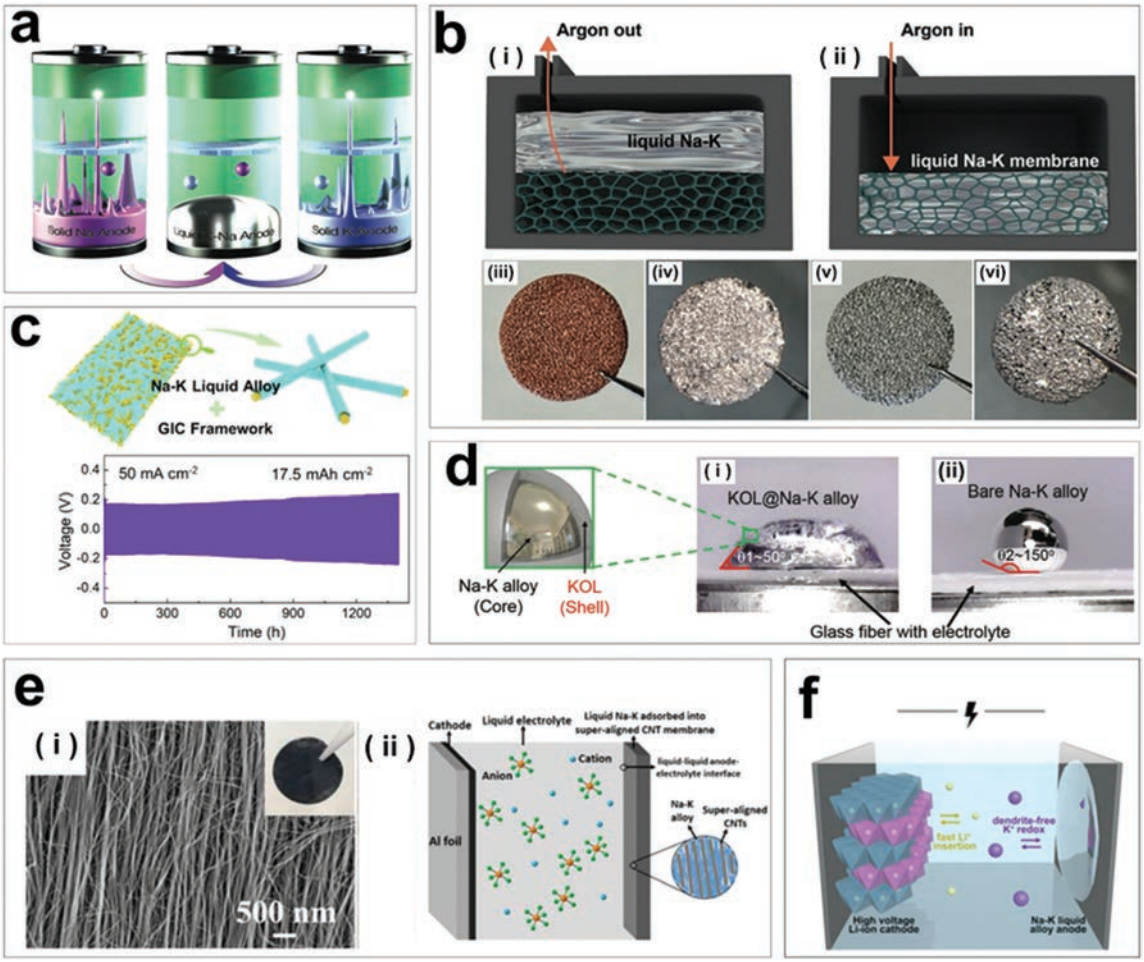

Fig. 11 (a) Schematic of a room-temperature Na–K alloy anode showing the advantages of self-healing and dendrite-free behaviours. For solid Na or K metals, serious dendrite growths can penetrate the separators and cause internal short-circuits.[107] (b) Vacuum infiltration of the Na–K alloy into various porous substrates (Cu/Al/Ni foams);[130] (c) stable cycling of the Na–K alloy absorbed onto a fibrous graphite substrate;[131] (d) photograph of liquid KOL@Na–K alloy (i) and liquid bare Na–K alloy (ii) on a glass fibre separator containing an organic liquid electrolyte (KPF6) at room temperature;[122] (e) (i) SEM and optical images of CM, and (ii) schematic of an anode with a liquid alloy adsorbed onto the CM;[132] (f) schematic of the ternary hybrid-cation LM battery.[133]

(K_2O) @Na–K liquid alloy consists of the Na–K liquid core and solid K_2O shell (Fig. 11d).[113] The K_2O not only serves as a protective layer to prevent the Na–K alloy from contacting the electrolyte but also greatly improves the wetting capability and adhesion between the liquid alloy and the carbon matrix (*e.g.* carbon fibre cloth (CFC)) to form a stable interface. Consequently, the as-prepared CFC/KOL@Na–K alloy anode exhibits good electrochemical performance with smaller hysteresis (less than 0.3 V beyond 140 cycles at 0.4 mA cm^{-2}), a better capacity retention, and a higher coulombic efficiency than the CFC/bare Na–K alloy. The room-temperature adsorption of liquid Na–K onto a super-aligned CNT membrane (CM) and flexible CM@NaK membrane have been shown (Fig. 11e).[132] The immiscibility of the Na–K alloy with liquid electrolyte enables the fabrication of electrodes comprising CM@NaK membranes with stable and dendrite-free anode-electrolyte (liquid–liquid) interfaces. An asymmetric K-ion capacitor (PIC) has been assembled using CM@NaK as the anode and activated carbon (AC) as the cathode. The PIC exhibits a high initial capacity of 94 mA h g^{-1} at 0.6 A g^{-1}, an excellent rate capability (82 mA h g^{-1} at 2.4 A g^{-1}), and long-term cyclic stability (63 mA h g^{-1} after 6000 cycles at 2.4 A g^{-1}), along with good energy/power density performance. A hybrid cationic LM battery configuration that inherits the advantages of both the LM and LIBs was fabricated (Fig. 11f).[133] This unique battery showed better cycling stability, comparable rate performance, and higher capacity compared to the Li-metal anode.

Like Ga-LM-based batteries, Na–K-LM-based batteries have high degrees of flexibility. An organic flexible Na–K battery that can operate as a SIB or K-ion battery has been proposed.[134] In this device, dibasic sodium rhodosonate (SR), an organic electroactive material, is used as the cathode and a stable hosted Na–K anode is fabricated using vacuum infiltration. The flexibilities of the liquid anode and organic cathode were used to successfully construct a flexible alkaline-ion

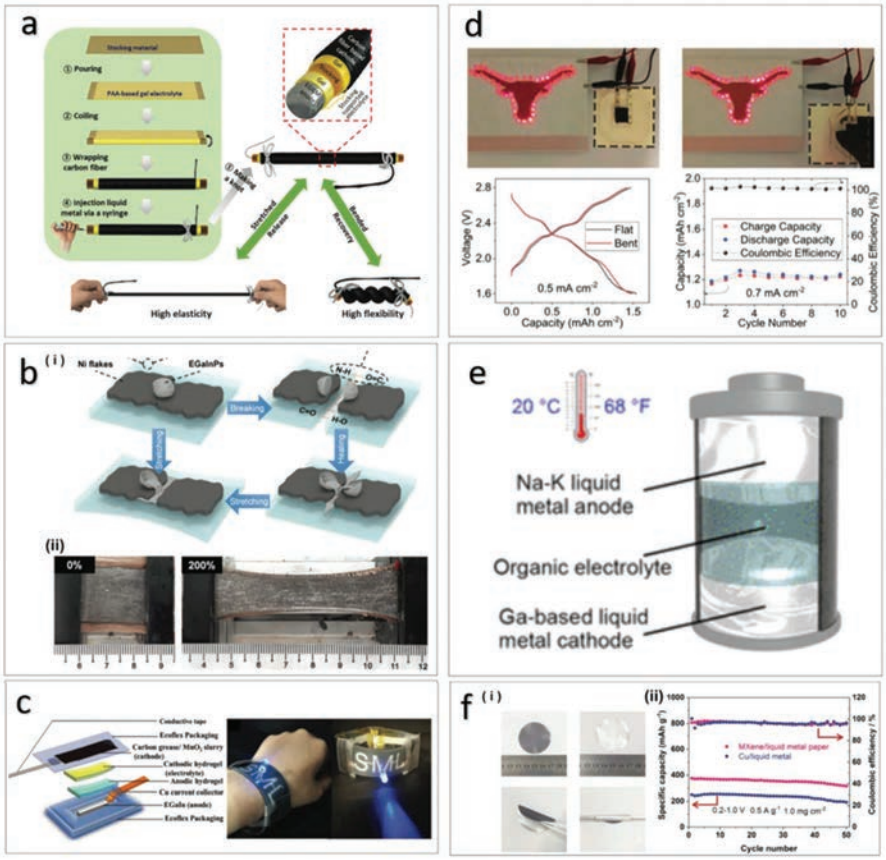

Fig. 12 (a) Sketch of the cable-shaped eutectic Ga–In LM–air battery: a simple and manoeuvrable preparation process and internal structure showing high flexibility and stretchability;[114] (b) An Ni flakes–EGaInPs–CPU conductor showing (i) the schematics of the mechanically and electrically stretchable and self-healing properties and (ii) different strains of the device;[115] (c) overview of a stretchable EGaIn–MnO_2 battery: composition of the battery, various views of the battery under undeformed and stretching/bending states, and a wristband demonstrated with two batteries in series for powering LEDs incorporated in a stretchable LM circuit;[116] (d) photographs of an organic flexible Na–K battery showing flat/bent states and battery performances as galvanostatic voltage profiles and cycling stabilities;[134] (e) schematic of a room-temperature LM battery;[25] (f) (i) optical image of MXene and MXene/LM papers, and (ii) cycling performances of MXene/LM paper and Cu/LM.[139]

battery with a capacity of up to 2.1 mA h cm^{-2} (Fig. 12d). This work demonstrated a robust room-temperature LM battery employing an Na–K alloy anode and Ga-based alloy cathode (Fig. 12e).[25] In the proof-of-concept cell test, the Ga–In-based LM battery maintained a capacity retention of 99.95% per cycle with a stabilised coulombic efficiency of ≈100%; similar electrochemical performances were also observed for Ga–Sn and galinstan-based LM batteries at room temperature. As described above, LMs with high flexibility and uniform elasticity have great potential as energy storage devices and can be applied to bendable and wearable electronic devices.

Conductive medium. The use of an LM as the conductive medium can also improve the degradation of the electrode by volume shrinkage and dendrite precipitation, while improving the cycling performance and capacity maintenance.

The Ga LM with sulfur (S) nanoparticles produces a uniform S–Ga core–shell structure (S@Ga) with an ultrathin shell of liquid Ga (Fig. 13a).[135] In this S@Ga composite, the thin Ga shell not only exhibits self-adaptive characteristics to perfectly adapt to the varying volume changes of S and restraining polysulfide shuttle, but also serves as a conductive agent to enhance electronic/ionic transmission, thereby improving the rate capacity of the S@Ga cathode. Therefore, the resultant S@Ga cathode exhibits a high capacity of 1295 mA h g^{-1} at 0.1C and high cycling stability with a small decay of 0.043% per cycle for 1000 cycles at 1C. A conductive, additive-free nanocomposite anode composed of LM and Si nanoparticles has been reported,[26] where the anode shows excellent electrochemical properties because the LMNPs improve electrode degradation owing to volume expansion and contraction of the Si nanoparticles during the electrochemical reactions (Fig. 13b). An anode made of lithium spinel titanate (LTO) mixed with GaSn LMNPs was proposed as a new composite material;[136] this composite anode improved the electrochemical properties of the LTO, showing better rate performance with a capacity of 115 mA h g^{-1} at 500 mA g^{-1} and excellent cycling stability with a reversible capacity of 135.6 mA h g^{-1} at 200 mA g^{-1} even after 1000 cycles. A novel self-healing artificial solid electrolyte interface (SEI) layer was successfully shown to protect the Li anode using a room-temperature

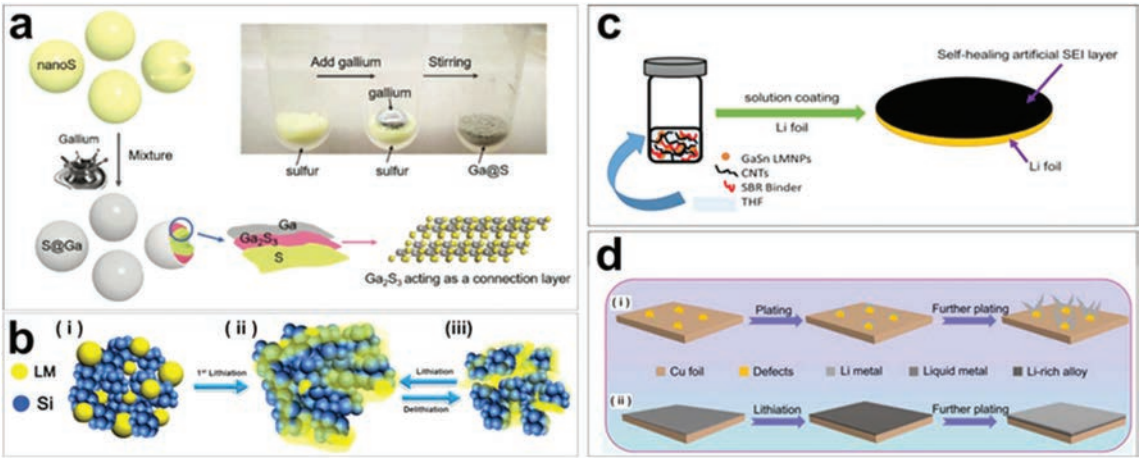

Fig. 13 (a) Schematic illustration of the fabrication process of S@Ga composites;[135] (b) scheme of the charge–discharge process of the LM/Si anode;[26] (c) schematic illustration of the fabrication of LMNP-Li anode;[137] (d) schematic showing the plating behaviours of Li on CF (i) and LCF (ii).[138]

Ga–Sn LM alloy (Fig. 13c).[137] In this artificial SEI layer, the LM not only regulates the Li^+ flux deposition uniformly but also avoids volume fluctuations that induce cracking of the SEI layer upon long-term cycling; hence, excellent full cell cycling performance can be achieved. Uniform Li deposition on metallic current collectors after coating with a thin 3 °C GaIn–Sn–Zinc (Zn) LM surface layer was reported.[138] The LM layer effectively lowers the nucleation barrier and inhibits growth of Li dendrites in the deposition process (Fig. 13d). LM can be applied as a conductive additive to improve the electrochemical properties of electrodes. The use of LM therefore enables the practical application of high-capacity alloy (*e.g.*, S and Si) anodes, which experience volume expansion and shrinkage problems, and Li-metal anodes, which have dendrite growth and SEI formation problems.

Owing to its high deformation ability, excellent electrical conductivity, and self-healing capability, LM is expected to be used in the next generation of energy devices for wearable products. For example, lightweight, flexible, freestanding, and binder-free MXene/LM paper can be fabricated by confining 3 °C GaIn–Sn–Zn LM in a paper matrix (Fig. 12f).[139] The resulting composite paper is foldable, bendable, and windable without shedding. When used as an anode for Li-ion cells, it exhibits satisfactory electrochemical performance.

Conclusion and future outlook

This paper presented a review of LMs as standalone nanoparticles and in conjunction with added nanoparticles in terms of applicable fabrication and applicational technologies, particularly those relevant to sensors, actuators, and batteries.

Easy and convenient fabrication of LMNPs can be achieved by ultrasonication, where the particle sizes are controllable. When LM-based materials are patterned for applications, the printing technique is typically used. LMNPs are also used for 3D wiring to maintain their shapes on the order of 10^{-6} m even when damaged. Because LMs have high surface tensions, it is difficult to maintain their shapes when damaged. However, when the LM is mixed with other nanoparticles, new properties and characteristics can be gained. For instance, LM combined with Fe is endowed with magnetic properties, and LM with Ag has increased conductivity. In other words, the properties of LM can be improved or newly acquired by addition of other materials with desirable properties.

For soft and flexible electronic device applications, different types of physical sensor can be fabricated using LMNCs, with improved mechanical properties such as magnetic sensing. Studies on LM show that they are essential components of soft and wearable electronics; thus, integrating LM with soft materials such as PDMS or Ecoflex produces flexible actuators with high electrical conductivities. Such soft robotic devices are generally desirable and feasible for use in drug delivery systems. When LMNPs or LMNCs are used as anodes in batteries, the battery capacities, stabilities, and rate performances are improved, whereas when used as conductive additives, the electrochemical properties are improved. LMNPs and LMNCs thus have a tremendous potential as innovative energy systems beyond the traditional all-solid and high-temperature batteries.

Further developments in flexible, stretchable, and wearable technologies can be achieved by adopting or advancing the unique properties of LM as well as by providing new properties to LMNC materials. In drug delivery or transportation systems, LMNPs and LMNC materials can have good effects on medical device applications; furthermore, many studies are being conducted on improving battery performances using LMs alone.

Even though LM has great potential in many applications, further development and improvements are needed. Na–K alloy-based anodes in batteries are good for avoiding dendrite problems but may cause safety issues when exposed to air or moisture. Hence, designing good batteries with a safe oper-

ation can be challenging. As for the Ga-based anode, improvement of properties other than capacity and volumetric density is needed.

The challenges concerning LMNPs may be highlighted as follows. (i) Conductivity improvement of LM particles as the current state of conductivity is suitable only for low-frequency devices, such as speaker cables; one of the methods to increase conductivity is by combining with silver. (ii) Merging LM particles—the mechanisms behind merging of various LM particles is not clear. (iii) Storage of LM particles must be investigated as they tend to oxidise over time. (iv) Reducing the sizes of LM particles is necessary for certain applications, such as drug delivery; the sizes of the particles can be controlled during sonication, but it is still a challenge to obtain small-sized particles in high concentrations. (v) LM contacts with other metals such as Ga are known to embrittle other metals; although there are cases where copper wires or graphene thin layers can be used as barriers, these are not studied in depth, which creates challenges in combining LM particles with other metals without barriers.

Conflicts of interest

There are no conflicts to declare.

Acknowledgements

This work was supported by the Japanese Science and Technology Agency, PRESTO Grant (Number: JPMJPR18J2), MIC/SCOPE (Number: 181603007) and research grant from Japan Keirin Autorace foundation (JKA).

References

1 Y. Lin, J. Genzer and M. D. Dickey, *Adv. Sci.*, 2020, **7**, 2000192.
2 M. H. Malakooti, M. R. Bockstaller, K. Matyjaszewskic and C. Majidi, *Nanoscale Adv.*, 2020, **2**, 2668–2677.
3 R. J. Whitney, *J. Physiol.*, 1953, **121**, 1–27.
4 N. B. Morley, J. Burris, L. C. Cadwallader and M. D. Nornberg, *Rev. Sci. Instrum.*, 2008, **79**, 056107.
5 M. J. Duggin, *Phys. Lett. A*, 1969, **29**, 470–471.
6 D. Zrnic and D. S. Swatik, *J. Less-Common Met.*, 1969, **18**, 67–68.
7 C. N. Cochran and L. M. Foster, *J. Electrochem. Soc.*, 1962, **109**, 144–148.
8 C. Pan, E. J. Markvicka, M. H. Malakooti, J. Yan, L. Hu, K. Matyjaszewski and C. Majidi, *Adv. Mater.*, 2019, **31**, 1900663.
9 S. Y. Tang, R. Qiao, Y. Lin, Y. Li, Q. Zhao, D. Yuan, G. Yun, J. Guo, M. D. Dickey, T. J. Huang, T. P. Davis, K. Kalantar-Zadeh and W. Li, *Adv. Mater. Technol.*, 2019, **4**, 1800420.
10 M. D. Dickey, *ACS Appl. Mater. Interfaces*, 2014, **6**(21), 18369–18379.
11 M. R. Khan, C. B. Eaker, E. F. Bowden and M. D. Dickey, *Proc. Natl. Acad. Sci. U. S. A.*, 2014, **111**(39), 14047–14051.
12 J. Yan, Y. Lu, G. Chen, M. Yang and Z. Gu, *Chem. Soc. Rev.*, 2018, **47**, 2518–2533.
13 F. P. Fehlner and N. F. Mott, *Oxid. Met.*, 1970, **2**, 59–99.
14 A. Martin, C. Du, B. Chang and M. Thuo, *Chem. Mater.*, 2020, **32**(21), 9045–9055.
15 L. Cademartiri, M. M. Thuo, C. A. Nijhuis, W. F. Reus, S. Tricard, J. R. Barber, R. N. S. Sodhi, P. Brodersen, C. Kim, R. C. Chiechi and G. M. Whitesides, *J. Phys. Chem. C*, 2012, **116**(20), 10848–10860.
16 A. Yamaguchi, Y. Mashima and T. Iyoda, *Angew. Chem., Int. Ed.*, 2015, **54**, 12809–12813.
17 H. Song, T. Kim, S. Kang, H. Jin, K. Lee and H. J. Yoon, *Small*, 2020, **16**, 1903391.
18 Y. Yu, Q. Wang, L. Yi and J. Liu, *Adv. Eng. Mater.*, 2014, **16**, 255–262.
19 J. Tang, X. Zhao, J. Li, R. Guo, Y. Zhou and J. Liu, *ACS Appl. Mater. Interfaces*, 2017, **9**(41), 35977–35987.
20 Y. Yang, J. Han, J. Huang, J. Sun, Z. L. Wang, S. Seo and Q. Sun, *Adv. Funct. Mater.*, 2020, **30**, 1909652.
21 R. Guo, X. Wang, H. Chang, W. Yu, S. Liang, W. Rao and J. Liu, *Adv. Eng. Mater.*, 2018, **20**, 1800054.
22 Y. G. Park, H. Min, H. Kim, A. Zhexembekova, C. Y. Lee and J. U. Park, *Nano Lett.*, 2019, **19**(8), 4866–4872.
23 J. Xu, Z. Wang, J. You, X. Li, M. Li, X. Wu and C. Li, *Chem. Eng. J.*, 2020, **392**, 123788.
24 K. Matsubara, D. Tachibana, R. Matsuda, H. Onoe, O. Fuchiwaki and H. Ota, *Adv. Intell. Syst.*, 2020, **2**, 2000008.
25 Y. Ding, X. Guo, Y. Qian, L. Xue, A. Dolocan and G. Yu, *Adv. Mater.*, 2020, **32**, 2002577.
26 B. Han, Y. Yang, X. Shi, G. Zhang, L. Gong, D. Xu, H. Zeng, C. Wang, M. Gu and Y. Deng, *Nano Energy*, 2018, **50**, 359–366.
27 R. Tutika, S. Kmiec, A. B. M. Tahidul Haque, S. W. Martin and M. D. Bartlett, *ACS Appl. Mater. Interfaces*, 2019, **11**(19), 17873–17883, DOI: 10.1021/acsami.9b04569.
28 J. Tang, X. Zhao, J. Li, Y. Zhou and J. Liu, *Adv. Sci.*, 2017, **4**, 1700024.
29 T. Daeneke, K. Khoshmanesh, N. Mahmood, I. A. de Castro, D. Esrafilzadeh, S. J. Barrow, M. D. Dickey and K. Kalantar-zadeh, *Chem. Soc. Rev.*, 2018, **47**, 4073–4111.
30 J. N. Hohman, M. Kim, G. A. Wadsworth, H. R. Bednar, J. Jiang, M. A. LeThai and P. S. Weiss, *Nano Lett.*, 2011, **11**(12), 5104–5110.
31 T. R. Lear, S. H. Hyun, J. W. Boley, E. L. White, D. H. Thompson and R. K. Kramer, *Extreme Mech. Lett.*, 2017, **13**, 126–134.
32 L. Ren, J. Zhuang, G. Casillas, H. Feng, Y. Liu, X. Xu, Y. Liu, J. Chen, Y. Du, L. Jiang and S. X. Dou, *Adv. Funct. Mater.*, 2016, **26**, 8111–8118.
33 J. Yan, X. Zhang, Y. Liu, Y. Ye, J. Yu, Q. Chen, J. Wang, Y. Zhang, Q. Hu, Y. Kang, M. Yang and Z. Gu, *Nano Res.*, 2019, **12**, 1313–1320.
34 I. D. Tevis, L. B. Newcomb and M. Thuo, *Langmuir*, 2014, **30**(47), 14308–14313.

35 S. Çınar, I. D. Tevis, J. Chen and M. Thuo, *Sci. Rep.*, 2016, **6**, 21864.
36 A. Martin, B. S. Chang, Z. Martin, D. Paramanik, C. Frankiewicz, S. Kundu, I. D. Tevis and M. Thuo, *Adv. Funct. Mater.*, 2019, **29**, 1903687.
37 B. S. Chang, R. Tutika, J. Cutinho, S. Oyola-Reynoso, J. Chen, M. D. Bartlett and M. M. Thuo, *Mater. Horiz.*, 2018, **5**, 416–422.
38 A. Martin, C. Du, A. M. Pauls, T. Ward and M. Thuo, *Adv. Mater. Interfaces*, 2020, **7**, 2001294.
39 B. S. Chang, M. Fratzl, A. Boyer, A. Martin, H. C. Ahrenholtz, I. D. Moraes, J. F. Bloch, N. M. Dempsey and M. M. Thuo, *Ind. Eng. Chem. Res.*, 2019, **58**(10), 4137–4142.
40 J. J. Chang, A. Martin, C. Du, A. M. Pauls and M. Thuo, *Angew. Chem., Int. Ed.*, 2020, **59**, 16346–16351.
41 G. Bo, L. Ren, X. Xu, Y. Du and S. Dou, *Adv. Phys.: X*, 2018, **3**, 1446359.
42 I. A. De Castro, A. F. Chrimes, A. Zavabeti, K. J. Berean, B. J. Carey, J. Zhuang, Y. Du, S. X. Dou, K. Suzuki, R. A. Shanks, R. Nixon-Luke, G. Bryant, K. Khoshmanesh, K. Kalantar-Zadeh and T. Daeneke, *Nano Lett.*, 2017, **17**(12), 7831–7838, DOI: 10.1021/acs.nanolett.7b04050.
43 B. Ma, C. Xu, J. Chi, J. Chen, C. Zhao and H. Liu, *Adv. Funct. Mater.*, 2019, **29**, 1901370.
44 A. Hirsch, H. O. Michaud, A. P. Gerratt, S. de Mulatier and S. P. Lacour, *Adv. Mater.*, 2016, **28**, 4507–4512.
45 M. Tavakoli, M. H. Malakooti, H. Paisana, Y. Ohm, D. G. Marques, P. A. Lopes, A. P. Piedade, A. T. de Almeida and C. Majidi, *Adv. Mater.*, 2018, **30**, 1801852.
46 L. Hu, H. Wang, X. Wang, X. Liu, J. Guo and J. Liu, *ACS Appl. Mater. Interfaces*, 2019, **11**(8), 8685–8692.
47 M. D. Bartlett, N. Kazem, M. J. Powell-Palm, X. Huang, W. Sun, J. A. Malen and C. Majidi, *Proc. Natl. Acad. Sci. U. S. A.*, 2017, **114**(9), 2143–2148.
48 F. Yu, J. Xu, H. Li, Z. Wang, L. Sun, T. Deng, P. Tao and Q. Liang, *Prog. Nat. Sci.: Mater. Int.*, 2018, **28**, 28–33.
49 I. D. Joshipura, H. R. Ayers, C. Majidi and M. D. Dickey, *J. Mater. Chem. C*, 2015, **3**, 3834–3841.
50 R. Guo, X. Sun, S. Yao, M. Duan, H. Wang, J. Liu and Z. Deng, *Adv. Mater. Technol.*, 2019, **4**, 1900183.
51 U. Daalkhaijav, O. D. Yirmibesoglu, S. Walker and Y. Mengüç, *Adv. Mater. Technol.*, 2018, **3**, 1700351.
52 R. Guo, H. Wang, X. Sun, S. Yao, H. Chang, H. Wang, J. Liu and Y. Zhang, *ACS Appl. Mater. Interfaces*, 2019, **11**, 30019–30027.
53 R. Zhao, R. Guo, X. Xu and J. Liu, *ACS Appl. Mater. Interfaces*, 2020, **12**(32), 36723–36730.
54 R. Guo, X. Sun, B. Yuan, H. Wang and J. Liu, *Adv. Sci.*, 2019, **6**, 1901478.
55 Z. Yu, F. F. Yun and X. Wang, *Mater. Horiz.*, 2018, **5**, 36–40.
56 M. G. Mohammed and R. Kramer, *Adv. Mater.*, 2017, **29**, 1604965.
57 L. Yang, X. Zhao, S. Xu, Y. Lu, H. Chang and J. Liu, *Sci. China: Technol. Sci.*, 2020, **63**, 289–296.
58 S. Liu, S. N. Reed, M. J. Higgins, M. S. Titus and R. K. Bottiglio, *Nanoscale*, 2019, **11**, 17615–17629.
59 A. Martin, W. Kiarie, B. Chang and M. Thuo, *Angew. Chem., Int. Ed.*, 2020, **59**, 352–357.
60 J. W. Boley, E. L. White and R. K. Kramer, *Adv. Mater.*, 2015, **27**, 2355–2360.
61 S. Liu, M. C. Yuen, E. L. White, J. W. Boley, B. Deng, G. J. Cheng and R. Kramer-Bottiglio, *ACS Appl. Mater. Interfaces*, 2018, **10**, 28232–28241.
62 B. Deng and G. J. Cheng, *Adv. Mater.*, 2019, **31**, 1807811.
63 X. Li, M. Li, J. Xu, J. You, Z. Yang and C. Li, *Nat. Commun.*, 2019, **10**, 3514.
64 Y. Lin, C. Cooper, M. Wang, J. J. Adams, J. Genzer and M. D. Dickey, *Small*, 2015, **11**, 6397–6403.
65 A. F. Silva, H. Paisana, T. Fernandes, J. Góis, A. Serra, J. F. J. Coelho, A. T. de Almeida, C. Majidi and M. Tavakoli, *Adv. Mater. Technol.*, 2020, **5**, 2000343.
66 L. Y. Zhou, J. Z. Fu, Q. Gao, P. Zhao and Y. He, *Adv. Funct. Mater.*, 2020, **30**, 1906683.
67 H. Chang, P. Zhang, R. Guo, Y. Cui, Y. Hou, Z. Sun and W. Rao, *ACS Appl. Mater. Interfaces*, 2020, **12**(12), 14125–14135.
68 A. Fassler and C. Majidi, *Adv. Mater.*, 2015, **27**, 1928–1932.
69 J. H. Oh, J. Y. Woo, S. Jo and C. S. Han, *Sens. Actuators, A*, 2019, **299**, 111610.
70 Y. Yang, J. Han, J. Huang, J. Sun, Z. L. Wang, S. Seo and Q. Sun, *Adv. Funct. Mater.*, 2020, **30**, 1909652.
71 S. Nayak, Y. Li, W. Tay, E. Zamburg, D. Singh, C. Lee, S. J. A. Koh, P. Chia and A. V. Y. Thean, *Nano Energy*, 2019, **64**, 103912.
72 Y. Mengüç, Y. L. Park, H. Pei, D. Vogt, P. M. Aubin, E. Winchell, L. Fluke, L. Stirling, R. J. Wood and C. J. Walsh, *Int. J. Robot. Res.*, 2014, **33**, 1748–1764.
73 S. Cheng and Z. Wu, *Adv. Funct. Mater.*, 2011, **21**, 2282–2290.
74 Y. Gao, H. Ota, E. W. Schaler, K. Chen, A. Zhao, W. Gao, H. M. Fahad, Y. Leng, A. Zheng, F. Xiong, C. Zhang, L. C. Tai, P. Zhao, R. S. Fearing and A. Javey, *Adv. Mater.*, 2017, **29**, 1701985.
75 T. Kozaki, S. Saito, Y. Otsuki, R. Matsuda, Y. Isoda, T. Endo, F. Nakamura, T. Araki, T. Furukawa, S. Maruo, M. Watanabe, K. Ueno and H. Ota, *Adv. Electron. Mater.*, 2020, **6**, 1901135.
76 X. Wang, R. Guo, B. Yuan, Y. Yao, F. Wang and J. Liu, *Annu. Int. Conf. IEEE Eng. Med. Biol. Soc. (EMBS)*, 2018, pp. 3276–3279.
77 J. Guo, W. Yang and C. Wang, *Adv. Mater.*, 2013, **25**, 5196–5214.
78 M. Molazemi, H. Shokrollahi and B. Hashemi, *J. Magn. Magn. Mater.*, 2013, **346**, 107–112.
79 R. Ito, G. Dodbiba and T. Fujita, *Int. J. Mod. Phys. B*, 2005, **19**, 1430–1436.
80 G. Dodbiba, K. Ono, H. S. Park, S. Matsuo and T. Fujita, *Electro-Rheological Fluids Magneto-Rheological Suspens. - Proc. 12th Int. Conf*, 2011, pp. 329–337.
81 M. Xiong, Y. Gao and J. Liu, *J. Magn. Magn. Mater.*, 2014, **354**, 279–283.

82 T. Fujita, H. S. Park, K. Ono, S. Matsuo, K. Okaya and G. Dodbiba, *J. Magn. Magn. Mater.*, 2011, **323**, 1207–1210.
83 C. Yang, X. Bian, J. Qin, T. Guo and X. Zhao, *RSC Adv.*, 2014, **4**, 59541–59547.
84 Q. Gao, H. Li, J. Zhang, Z. Xie, J. Zhang and L. Wang, *Sci. Rep.*, 2019, **9**, 5908.
85 Y. L. Park, B. R. Chen and R. J. Wood, *IEEE Sens. J.*, 2012, **12**, 2711–2718.
86 T. Hu, S. Xuan, L. Ding and X. Gong, *Sens. Actuators, B*, 2020, **314**, 128095.
87 G. Yun, S. Y. Tang, S. Sun, D. Yuan, Q. Zhao, L. Deng, S. Yan, H. Du, M. D. Dickey and W. Li, *Nat. Commun.*, 2019, **10**, 1300.
88 D. H. Kim and J. A. Rogers, *Adv. Mater.*, 2008, **20**, 4887–4892.
89 K. Sim, Z. Rao, F. Ershad and C. Yu, *Adv. Mater.*, 2020, **32**, 1902417.
90 M. Woo, *Proc. Natl. Acad. Sci. U. S. A.*, 2020, **117**(10), 5088–5091.
91 S. Zhu, J. H. So, R. Mays, S. Desai, W. R. Barnes, B. Pourdeyhimi and M. D. Dickey, *Adv. Funct. Mater.*, 2013, **23**, 2308–2314, DOI: 10.1002/adfm.201202405.
92 B. Yao, W. Hong, T. Chen, Z. Han, X. Xu, R. Hu, J. Hao, C. Li, H. Li, S. E. Perini, M. T. Lanagan, S. Zhang, Q. Wang and H. Wang, *Adv. Mater.*, 2020, **32**, 1907499.
93 M. D. Bartlett, A. Fassler, N. Kazem, E. J. Markvicka, P. Mandal and C. Majidi, *Adv. Mater.*, 2016, **28**, 3726–3731.
94 H. Wang, Y. Yao, Z. He, W. Rao, L. Hu, S. Chen, J. Lin, J. Gao, P. Zhang, X. Sun, X. Wang, Y. Cui, Q. Wang, S. Dong, G. Chen and J. Liu, *Adv. Mater.*, 2019, **31**, 1901337.
95 M. H. Malakooti, N. Kazem, J. Yan, C. Pan, E. J. Markvicka, K. Matyjaszewski and C. Majidi, *Adv. Funct. Mater.*, 2019, **29**, 1906098.
96 M. Zadan, M. H. Malakooti and C. Majidi, *ACS Appl. Mater. Interfaces*, 2020, **12**(15), 17921–17928.
97 E. J. Markvicka, M. D. Bartlett, X. Huang and C. Majidi, *Nat. Mater.*, 2018, **17**, 618–624.
98 M. G. Saborio, S. Cai, J. Tang, M. B. Ghasemian, M. Mayyas, J. Han, M. J. Christoe, S. Peng, P. Koshy, D. Esrafilzadeh, R. Jalili, C. H. Wang and K. Kalantar-Zadeh, *Small*, 2020, **16**, 1903753.
99 Y. Lu, Q. Hu, Y. Lin, D. B. Pacardo, C. Wang, W. Sun, F. S. Ligler, M. D. Dickey and Z. Gu, *Nat. Commun.*, 2015, **6**, 10066.
100 Y. Lu, Y. Lin, Z. Chen, Q. Hu, Y. Liu, S. Yu, W. Gao, M. D. Dickey and Z. Gu, *Nano Lett.*, 2017, **17**, 2138–2145.
101 A. Elbourne, S. Cheeseman, P. Atkin, N. P. Truong, N. Syed, A. Zavabeti, M. Mohiuddin, D. Esrafilzadeh, D. Cozzolino, C. F. McConville, M. D. Dickey, R. J. Crawford, K. Kalantar-Zadeh, J. Chapman, T. Daeneke and V. K. Truong, *ACS Nano*, 2020, **14**(1), 802–817.
102 K. Khoshmanesh, S. Y. Tang, J. Y. Zhu, S. Schaefer, A. Mitchell, K. Kalantar-Zadeh and M. D. Dickey, *Lab Chip*, 2017, **17**, 974–993.
103 X. Guo, L. Zhang, Y. Ding, J. B. Goodenough and G. Yu, *Energy Environ. Sci.*, 2019, **12**, 2605–2619.
104 U. Gulzar, S. Goriparti, E. Miele, T. Li, G. Maidecchi, A. Toma, F. De Angelis, C. Capiglia and R. P. Zaccaria, *J. Mater. Chem. A*, 2016, **4**, 16771–16800.
105 H. Kim, D. A. Boysen, J. M. Newhouse, B. L. Spatocco, B. Chung, P. J. Burke, D. J. Bradwell, K. Jiang, A. A. Tomaszowska, K. Wang, W. Wei, L. A. Ortiz, S. A. Barriga, S. M. Poizeau and D. R. Sadoway, *Chem. Rev.*, 2013, **113**(3), 2075–2099.
106 Y. Ding, Y. Zhao and G. Yu, *Nano Lett.*, 2015, **15**(6), 4108–4113.
107 L. Xue, H. Gao, W. Zhou, S. Xin, K. Park, Y. Li and J. B. Goodenough, *Adv. Mater.*, 2016, **28**, 9608–9612.
108 A. Zavabeti, J. Z. Ou, B. J. Carey, N. Syed, R. Orrell-Trigg, E. L. H. Mayes, C. Xu, O. Kavehei, A. P. O'Mullane, R. B. Kaner, K. Kalantar-Zadeh and T. Daeneke, *Science*, 2017, **358**, 332–335.
109 R. D. Deshpande, J. Li, Y.-T. Cheng and M. W. Verbrugge, *J. Electrochem. Soc.*, 2011, **158**, A845.
110 J. Saint, M. Morcrette, D. Larcher and J. M. Tarascon, *Solid State Ionics*, 2005, **176**, 189–197.
111 T. Gancarz, *J. Mol. Liq.*, 2017, **241**, 231–236.
112 Y. Wu, L. Huang, X. Huang, X. Guo, D. Liu, D. Zheng, X. Zhang, R. Ren, D. Qu and J. Chen, *Energy Environ. Sci.*, 2017, **10**, 1854–1861.
113 X. Guo, Y. Ding, L. Xue, L. Zhang, C. Zhang, J. B. Goodenough and G. Yu, *Adv. Funct. Mater.*, 2018, **28**, 1804649.
114 G. Liu, J. Y. Kim, M. Wang, J. Y. Woo, L. Wang, D. Zou and J. K. Lee, *Adv. Energy Mater.*, 2018, **8**, 1703652.
115 S. Park, G. Thangavel, K. Parida, S. Li and P. S. Lee, *Adv. Mater.*, 2019, **31**, 1805536.
116 D. Liu, L. Su, J. Liao, B. Reeja-Jayan and C. Majidi, *Adv. Energy Mater.*, 2019, **9**, 1902798.
117 J. B. Goodenough and Y. Kim, *Chem. Mater.*, 2010, **22**, 587–603.
118 D. Lin, Y. Liu and Y. Cui, *Nat. Nanotechnol.*, 2017, **12**, 194–206.
119 R. Zhang, N. W. Li, X. B. Cheng, Y. X. Yin, Q. Zhang and Y. G. Guo, *Adv. Sci.*, 2017, **4**, 1600445.
120 L. Fan, K. Lin, J. Wang, R. Ma and B. Lu, *Adv. Mater.*, 2018, **30**, 1800804.
121 L. Fan, R. Ma, J. Wang, H. Yang and B. Lu, *Adv. Mater.*, 2018, **30**, 1805486.
122 L. Zhang, X. Xia, Y. Zhong, D. Xie, S. Liu, X. Wang and J. Tu, *Adv. Mater.*, 2018, **30**, 1804011.
123 J. Bae, Y. Li, J. Zhang, X. Zhou, F. Zhao, Y. Shi, J. B. Goodenough and G. Yu, *Angew. Chem., Int. Ed.*, 2018, **57**, 2096–2100.
124 G. Zheng, S. W. Lee, Z. Liang, H. W. Lee, K. Yan, H. Yao, H. Wang, W. Li, S. Chu and Y. Cui, *Nat. Nanotechnol.*, 2014, **9**, 618–623.
125 C. P. Yang, Y. X. Yin, S. F. Zhang, N. W. Li and Y. G. Guo, *Nat. Commun.*, 2015, **6**, 8058.
126 X. Lu, G. Li, J. Y. Kim, D. Mei, J. P. Lemmon, V. L. Sprenkle and J. Liu, *Nat. Commun.*, 2014, **5**, 4578.

127 Y. Jin, K. Liu, J. Lang, D. Zhuo, Z. Huang, C. Wang, H. Wu and Y. Cui, *Nat. Energy*, 2018, **3**, 732–738.
128 J. Liu, J. G. Zhang, Z. Yang, J. P. Lemmon, C. Imhoff, G. L. Graff, L. Li, J. Hu, C. Wang, J. Xiao, G. Xia, V. V. Viswanathan, S. Baskaran, V. Sprenkle, X. Li, Y. Shao and B. Schwenzer, *Adv. Funct. Mater.*, 2013, **23**, 929–946, DOI: 10.1002/adfm.201200690.
129 L. Xue, H. Gao, Y. Li and J. B. Goodenough, *J. Am. Chem. Soc.*, 2018, **140**, 3292–3298.
130 L. Xue, W. Zhou, S. Xin, H. Gao, Y. Li, A. Zhou and J. B. Goodenough, *Angew. Chem., Int. Ed.*, 2018, **57**, 14184–14187.
131 L. Zhang, S. Peng, Y. Ding, X. Guo, Y. Qian, H. Celio, G. He and G. Yu, *Energy Environ. Sci.*, 2019, **12**, 1989–1998.
132 L. Qin, W. Yang, W. Lv, L. Liu, Y. Lei, W. Yu, F. Kang, J. K. Kim, D. Zhai and Q. H. Yang, *Chem. Commun.*, 2018, **54**, 8032–8035.
133 X. Guo, Y. Ding, H. Gao, J. B. Goodenough and G. Yu, *Adv. Mater.*, 2020, **32**, 2000316.
134 Y. Ding, X. Guo, Y. Qian, L. Zhang, L. Xue, J. B. Goodenough and G. Yu, *Adv. Mater.*, 2019, **31**, 1806956.
135 M. Zhu, S. Li, B. Li and S. Yang, *Nanoscale*, 2019, **11**, 412–417.
136 Y. Liu, L. P. Yue, P. Lou, G. H. Xu, J. Liang, P. Guo, J. Wang, R. Tao, Y. C. Cao and L. Shi, *Mater. Lett.*, 2020, **258**, 126803.
137 G. Zhang, H. Deng, R. Tao, B. Xiao, T. Hou, S. Yue, N. Shida, Q. Cheng, W. Zhang and J. Liang, *Mater. Lett.*, 2020, **262**, 127194, DOI: 10.1016/J.MATLET.2019.127194.
138 C. Wei, H. Fei, Y. An, Y. Tao, J. Feng and Y. Qian, *J. Mater. Chem. A*, 2019, **7**, 18861–18870.
139 C. Wei, H. Fei, Y. Tian, Y. An, G. Zeng, J. Feng and Y. Qian, *Small*, 2019, **15**, 1903214.